19. Magnetic flux tubes. Sunspots.

Magnetic Flux Tubes. Sunspots.

- Observational Evidence for Flux Tubes.
- Concentrations of magnetic flux.
- Convective Collapse.
- Hydraulic Concentration.
- Magnetic Buoyancy.
- Sunspots.

Observational Evidence for Flux Tubes.

Sunspots are large tubes of magnetic flux. The smallest flux tubes visible in white light are pores which are as dark as sunspots but have no penumbra. Their size is of one or several granules. The lifetime is about 1 day. The magnetic field strength is about 1500 G or higher.

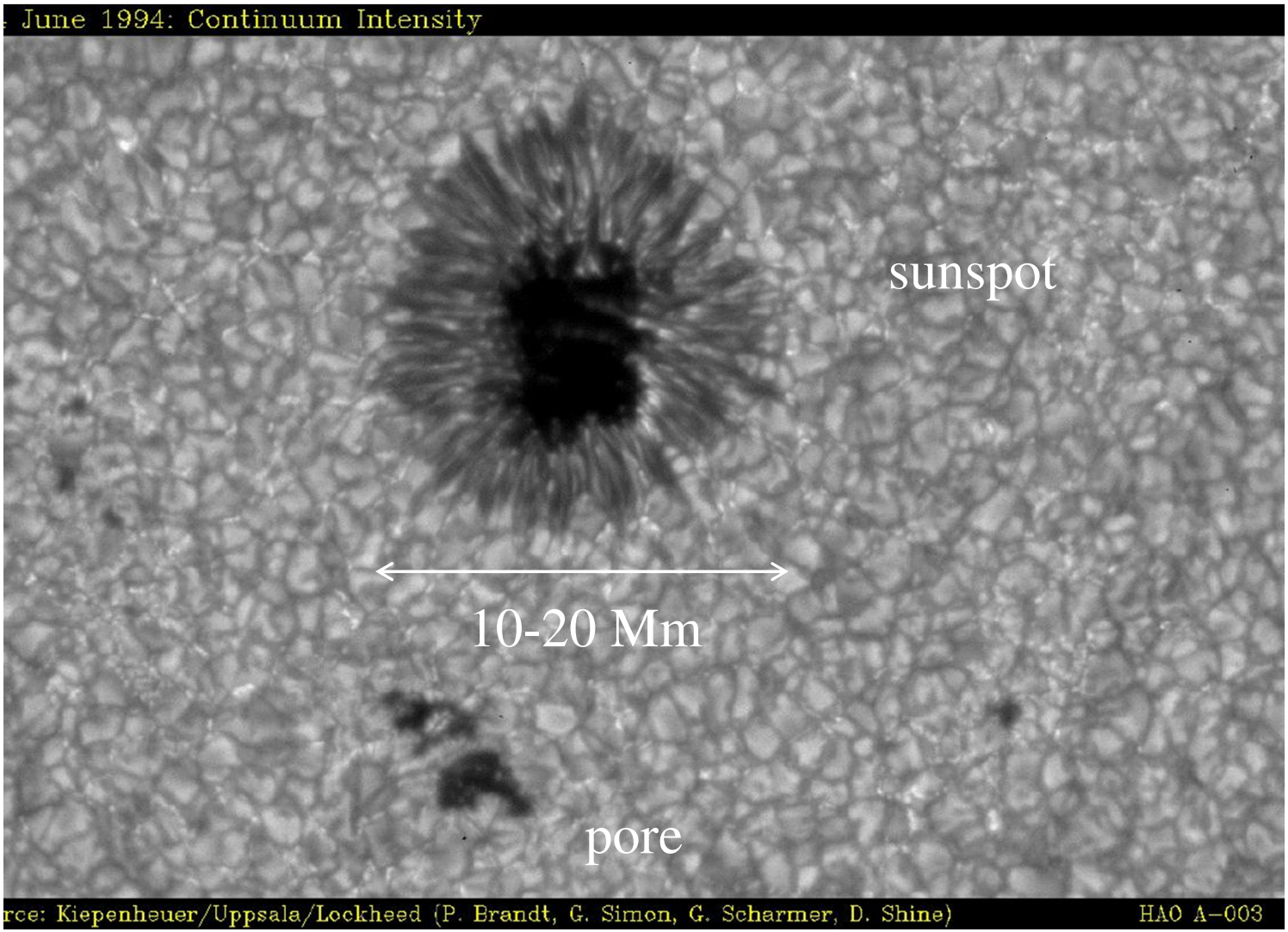

Magnetic knots are almost invisible in white light but seen in spectrograms because of Zeeman line broadening. Magnetic field is also about 1000-2000 G.

The small magnetic elements are observed in the so-called G-band, molecular CH line at 4300Å.

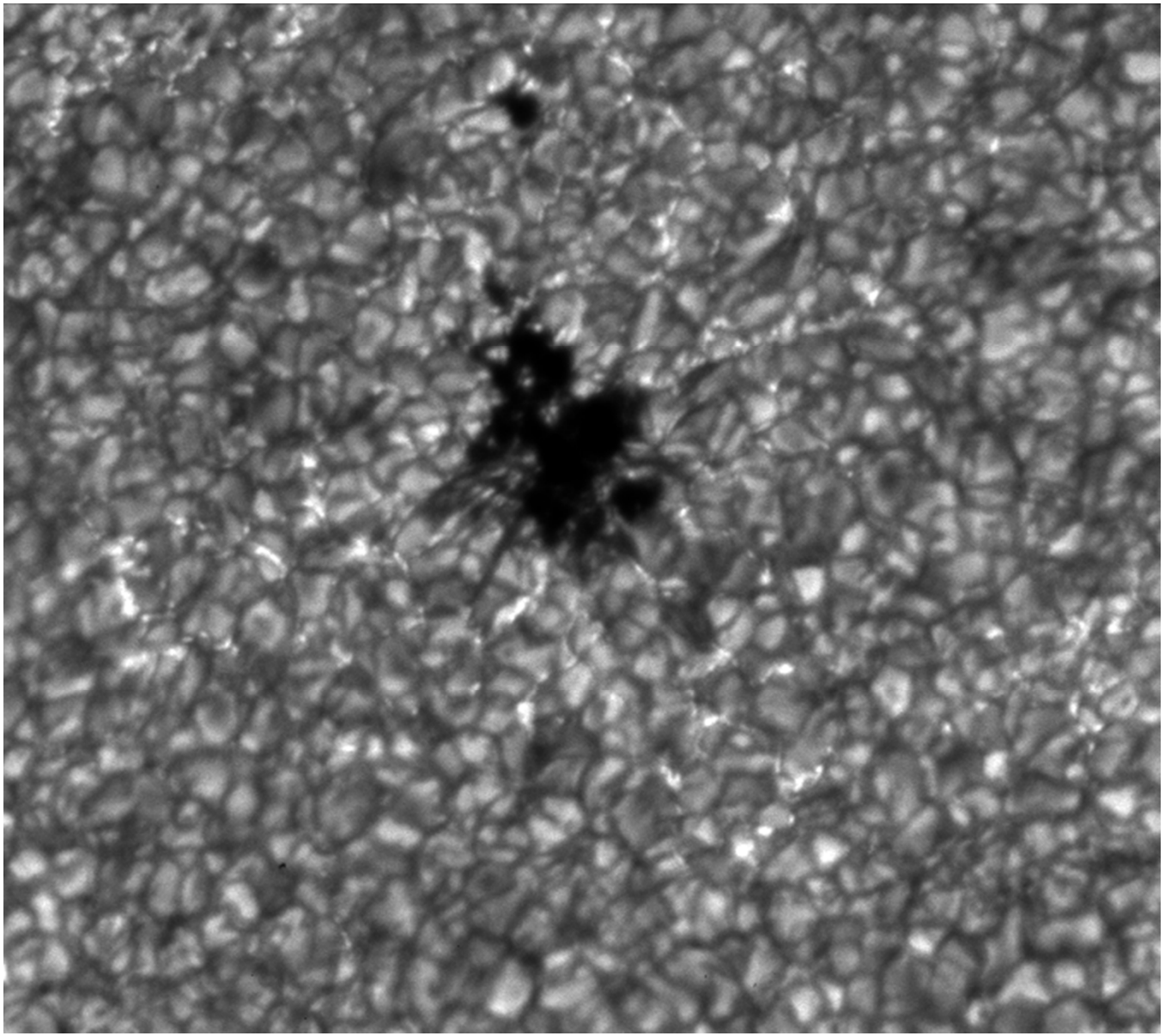

A filtergram at 4305Å (G-Band) taken with the Swedish Vacuum Solar Telescope on La Palma. The highly dynamical interaction between granular motions and magnetic elements in the solar photosphere can be observed at the limit of what current telescopes can resolve.

The average G-band contrast of magnetic elements shows no size dependency over a range of 150—600 km in diameter. G-band bright points occur without exception on sites of isolated magnetic flux concentrations or peninsular concentrations extending from larger concentrations of flux; isolated magnetic flux concentrations are found without associated G-band bright points.

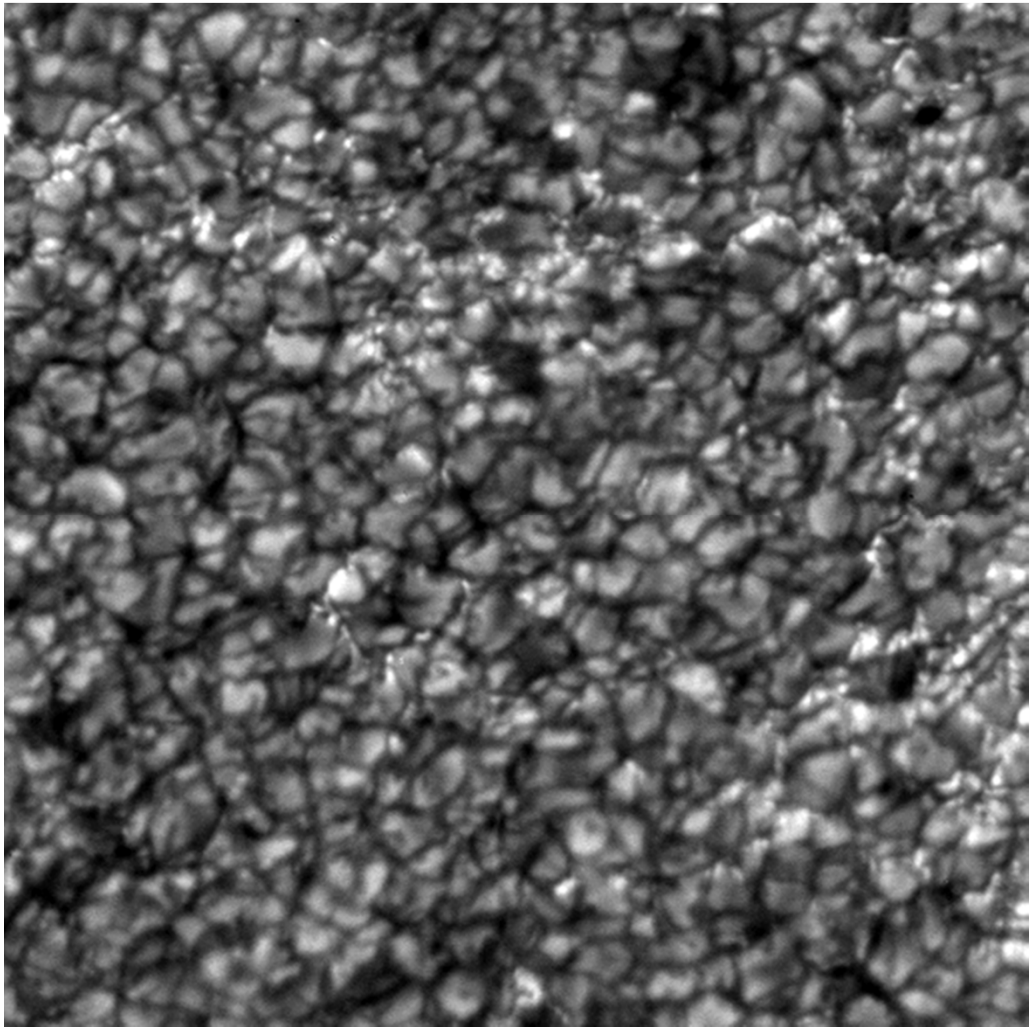

Magnetic elements demarcated by G-band bright points occupy no more than 1—2% of plage and active network regions by area at any one time. Magnetic elements move in the intergranular flow field at speeds from 0.5 to 5 km sec^{-1}. The RMS speed is 2.4 km sec^{-1} over an average range of 2100 km (3 arcsec). Continual fragmentation and merging of magnetic elements is the normal evolutionary mode for small-scale magnetic elements. The time scale for the dynamics is approximately 6–8 minutes, but significant morphological changes occur on time scales as short as 100 seconds.

High-resolution observations of small-scale magnetic elements

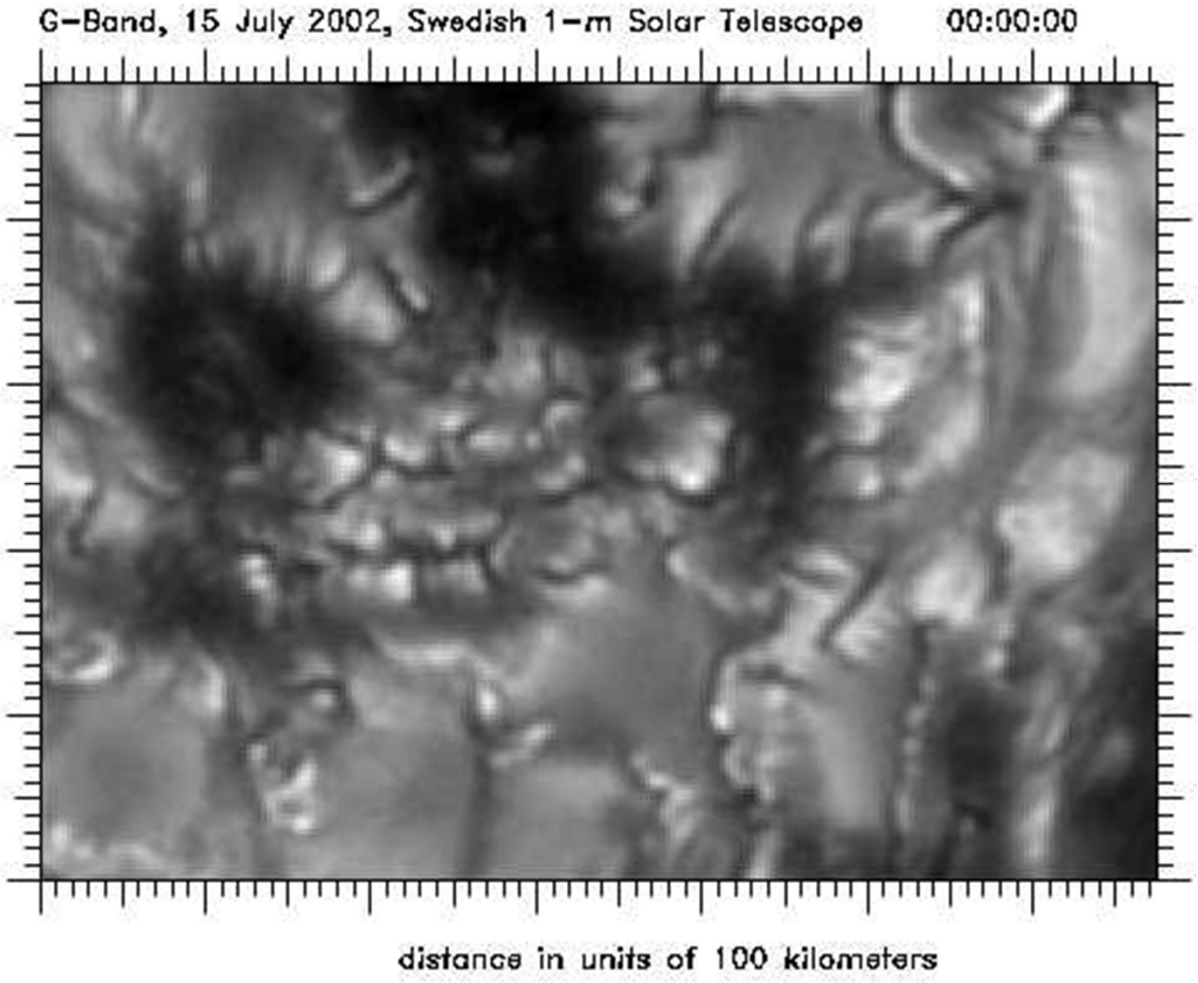

Small magnetic elements

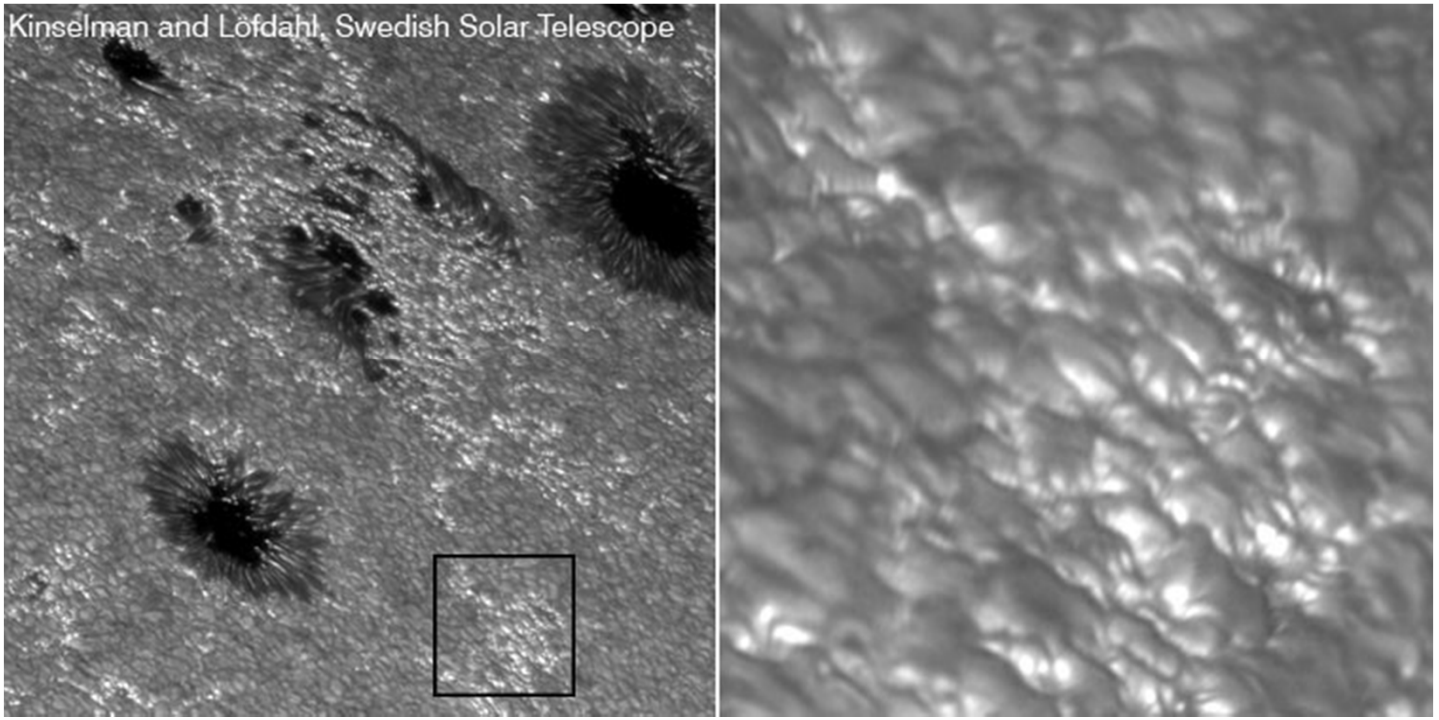

Small magnetic elements that constitute plages are brighter near the limb because we see "hot wall" in deeper layers (since density inside the flux tubes is lower the layer of optical depth 1.

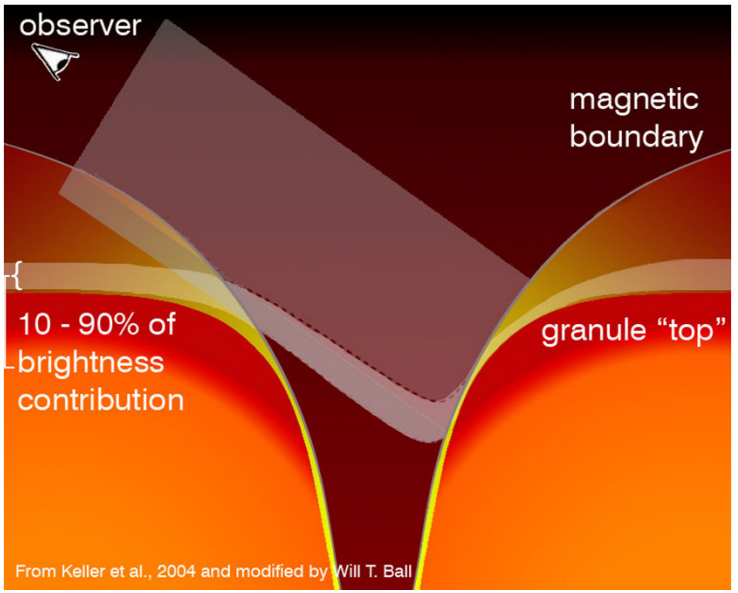

PHYSICAL ORIGIN OF THE G-BAND BRIGHTENING

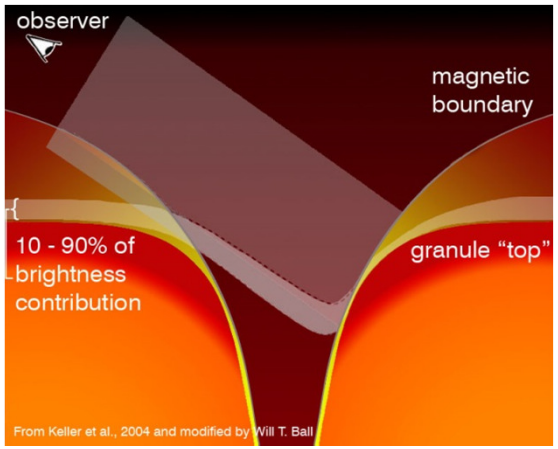

Why are the G-band bright points so closely associated with the magnetic flux concentrations in the downflow regions?

The enhanced G-band brightness of the granules is mostly due to their larger continuum intensity. While the magnetic elements also appear bright in the continuum radiation, their intensity contrast in the G band is much larger.

This is due to the strong weakening of the absorption in the CH lines due to the depletion of CH molecules in the magnetic flux concentrations by the combined effects of a larger temperature (higher dissociation rate) and a lower density (less associative collisions).

The much lower CH concentration at the formation height of the CH spectrum around leads to less absorption in the spectral lines of this molecule and thus, together with the higher level of continuum intensity, to a strongly increased brightness in the G band.

The physical association of a large field strength with a higher temperature and a lower density can easily be understood in terms of lateral heating by radiation of the transparent tenuous interior of a flux concentration in lateral balance of the total (gas plus magnetic) pressure. In fact, the strong flux concentrations in the simulations are found to be almost in total pressure equilibrium, showing values of the plasma beta (gas pressure divided by magnetic pressure) of the order of 0.1 around the average level of optical depth unity in the weakly magnetic part of the photosphere.

Number density of CH molecules vs the optical depth in magnetic elements with weak and strong magnetic field.

Strong magnetic field elements are bright in the G-band because the CH absorption is reduced.

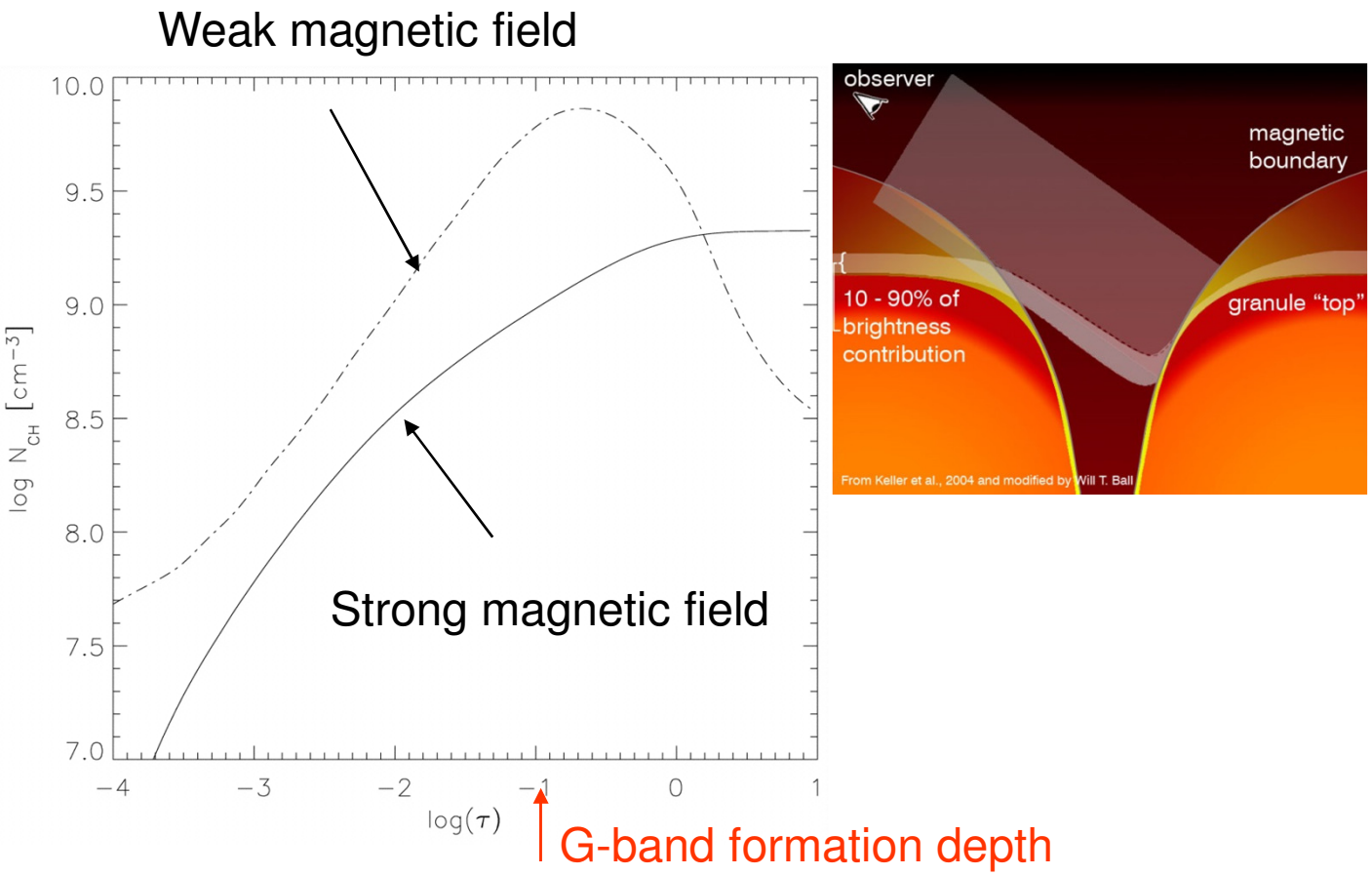

FIG. 3.—Number density of CH molecules, N_{CH}, as a function of continuum optical depth at 500 nm, τ. The dashed line corresponds to the average weakly magnetized ($B < 50$ G) atmosphere of the simulation snapshot shown in Fig. 1, and the solid line corresponds to the average atmosphere of the bright magnetic elements with a field strength above 1000 G and a G-band intensity above 1.5 of the average value. The CH lines in the G band are formed around $\log \tau = -1$. In this layer, the number density of CH is reduced by more than factor of 6 within the magnetic flux concentrations in comparison with the average atmosphere. This drop of the CH concentration is due to a 17% higher temperature (corresponding to about 900 K) and a 30% lower density within the magnetic flux concentration in the range of optical depth where the spectral lines of CH are formed. A low number density of CH leads to less absorption in the CH lines and thus larger G-band brightness.

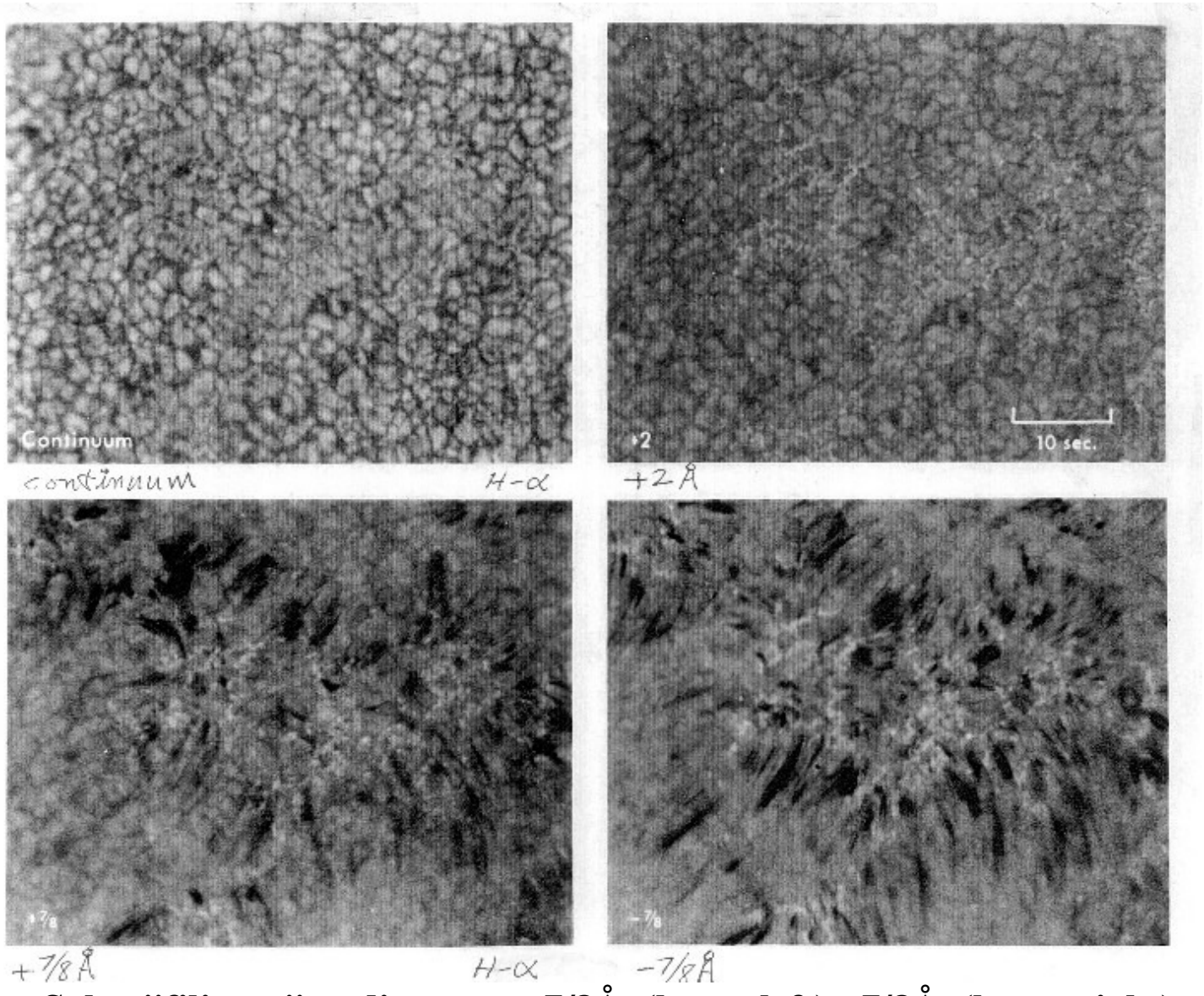

Solar "filigree" at distances +7/8Å (lower left), -7/8Å (lower right), and +2Å (upper right) from the center H_α. The corresponding continuum image is shown in upper left. A typical size of filigree is 0.25 arcsec (200 km). They are probably highly concentrated magnetic structures.

Concentrations of Magnetic Flux.

Flux concentrations can be produced by converging motions. Supergranular flow can be modeled by a hexagonal convective cells. At the bottom the flow converges at the center, and at the top converges at the six vertices. Each point of convergence marks columns of concentrated vertical field.

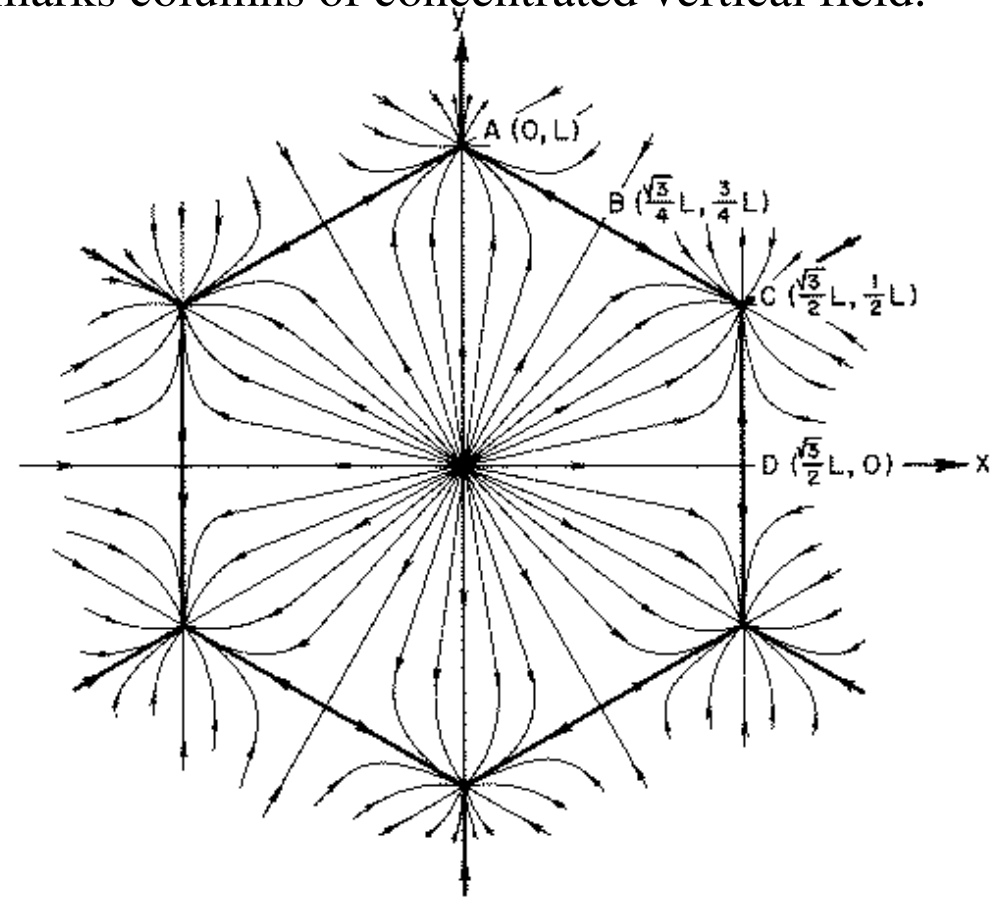

Streamlines at the top of hexagonal convective cells.

Estimate the size of magnetic elements

In the steady state the time scale of field decay, d^2/η must be equal to time scale of field advection into the columns, l/u, where d is the size of the elements, l is the size of convective cells, η is magnetic diffusivity, u is the convective velocity:

$$\frac{d^2}{\eta} = \frac{l}{u}.$$

Thus, $$d^2 = \frac{\eta l}{u},$$

or $d = \frac{l}{R_m^{1/2}}$, where $R_m = \frac{ul}{\eta}$ - magnetic Reynolds number.

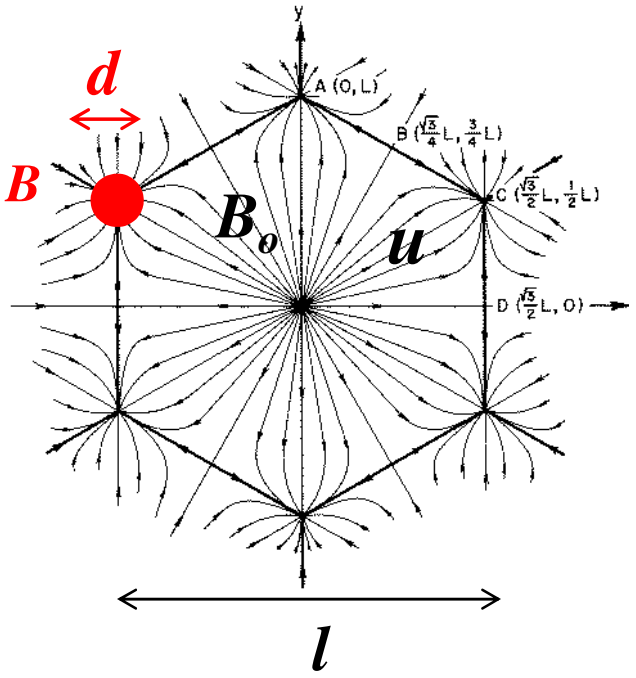

To estimate the field strength in the magnetic concentration we assume that the whole magnetic flux, $B_0 l^2$ across the convective cell is concentrated in the elements:

$$B_0 l^2 \simeq B d^2.$$

Therefore, inside a flux tube the magnetic field is: $B \simeq R_m B_0$.

Typical estimates: $l = 3\times10^9$ cm, $R_m = 10^4$, B_0 =0.1 G, then $d = 3\times10^7$ cm, $B = 10^3$ G.

Estimate the magnetic field strength

The field concentration is a very rapid process on the time scale of $l/u \simeq 10^5$ sec (1 day).

However, the field concentration stops when field becomes strong and resists motions, that is, when the magnetic pressure compares with the dynamic pressure:

$$\frac{B^2}{8\pi} \simeq \frac{\rho u^2}{2},$$

or

$$B \simeq \sqrt{8\pi\rho}u.$$

For photospheric conditions, $\rho = 3\times10^{-7}$ g/cm ^{3} , $u = 3\times10^4$ cm/s, $B \simeq 60$ G. This is smaller than the observed values.

Parker suggested that magnetic field is concentrated due to downflows along the flux tubes and external gas pressure.

Convective Collapse.

Consider a vertical flux tube in the convection zone (with a superadiabatic stratification).

A small adiabatic downward displacement makes the matter in the tube cool with respect to its (superadiabatic) surroundings. The reduced temperature enhanced the downdraft within the field and permits the gravitational field to evacuate the flux tube. The magnetic field is then strongly suppressed by external gas pressure, leading to extraordinary observed strengths of 1500 G or more.

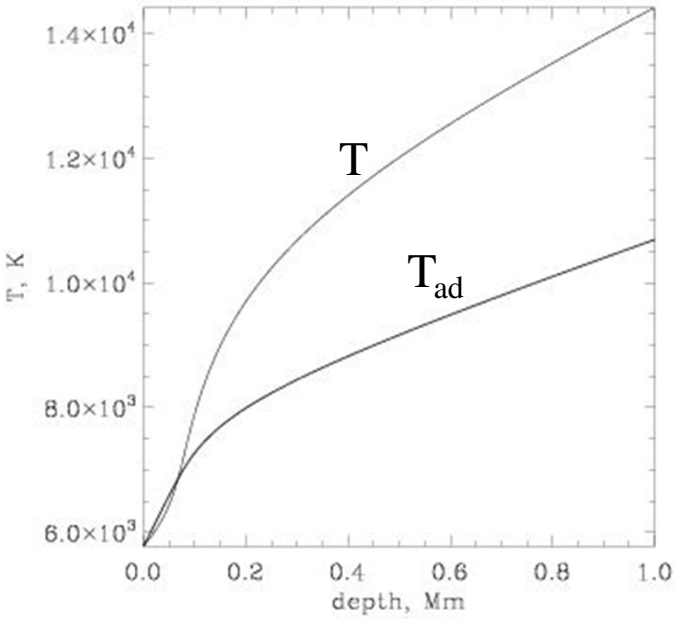

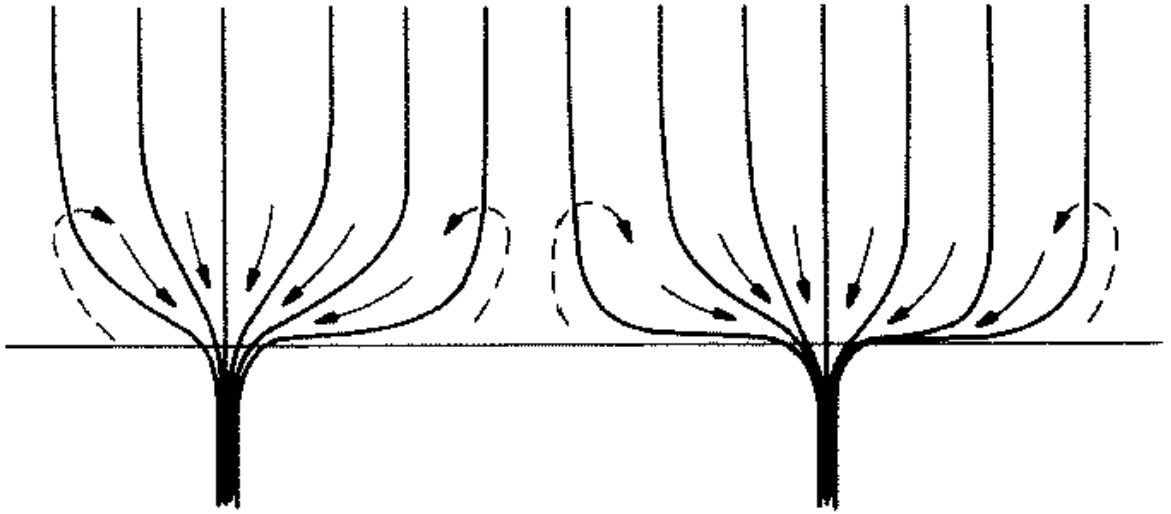

A sketch of the magnetic field of isolated concentrated flux tubes where there is a net magnetic flux through the surface of the Sun. The solid arrows represent the downdraft within the field. The dashed arrows are the conjectured upward flow supplying the downdraft.

Hydraulic Concentration of magnetic flux tubes

Consider a flux tube with axis x along the tube. The pressure balance across the tube is:

$$P = P_i + \frac{B^2}{8\pi},$$ where P_i is the internal pressure.

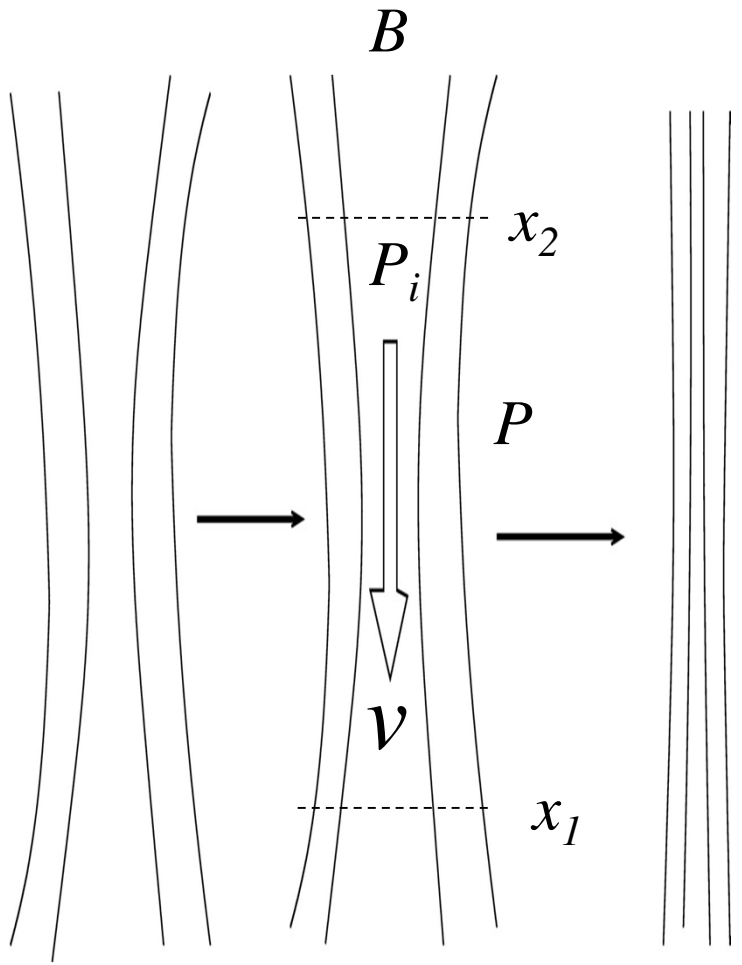

The momentum equation for a flow along the tube:

$$\frac{\partial v}{\partial t} + v\frac{\partial v}{\partial x} + \frac{1}{\rho}\frac{\partial P_i}{\partial x} = 0.$$

Substituting P_i from the first equation we obtain:

$$\frac{\partial v}{\partial t} + \frac{\partial}{\partial x}\left(\frac{1}{2}v^2 + \frac{P}{\rho} - \frac{B^2}{8\pi\rho}\right) = 0.$$

We integrate along the flux tube: $\int_{x_1}^{x_2} ...dx \equiv < ... >$

and consider a stationary flow: $\left\langle \partial v / \partial t \right\rangle = 0$:

$$\left\langle P + \frac{1}{2}\rho v^2 - \frac{B^2}{8\pi} \right\rangle = < P_i >,$$

Finally, we get: $\left\langle \frac{B^2}{8\pi} \right\rangle = \left\langle P \right\rangle + \frac{1}{2}\left\langle \rho v^2 \right\rangle - \left\langle P_i \right\rangle$. **Thus, the magnetic field inside the tube is increased by the external pressure and flow along the tube. The diameter of the flux tube is decreased because of the conservation of magnetic flux.**

Emerging flux tubes. Magnetic buoyancy.

Consider a horizontal flux tube in the convection zone without a flow.

The pressure balance: $P_e = P_i + \frac{B^2}{8\pi}$.

Using the equation of state $P = RT\rho$ we obtain:

$$RT(\rho_e - \rho_i) = \frac{B_i^2}{8\pi}.$$

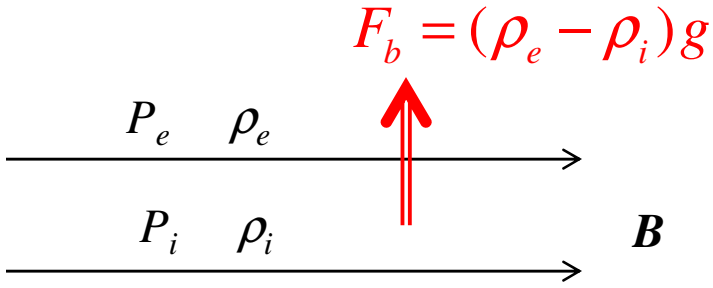

Thus, $\rho_i < \rho_e$, the density inside the tube is lower than in the surroundings, and there is a buoyancy force: $(\rho_e - \rho_i)g$.

When the buoyancy force is stronger than the magnetic tension force the flux tube becomes unstable. Estimate the tension force.
The Lorentz force has two components: magnetic pressure and tension force: $\mathbf{f} = \frac{(\nabla \times \mathbf{B}) \times \mathbf{B}}{4\pi} = \frac{(\mathbf{B}\cdot\nabla)\mathbf{B}}{4\pi} - \nabla\frac{\mathbf{B}^2}{8\pi}$.

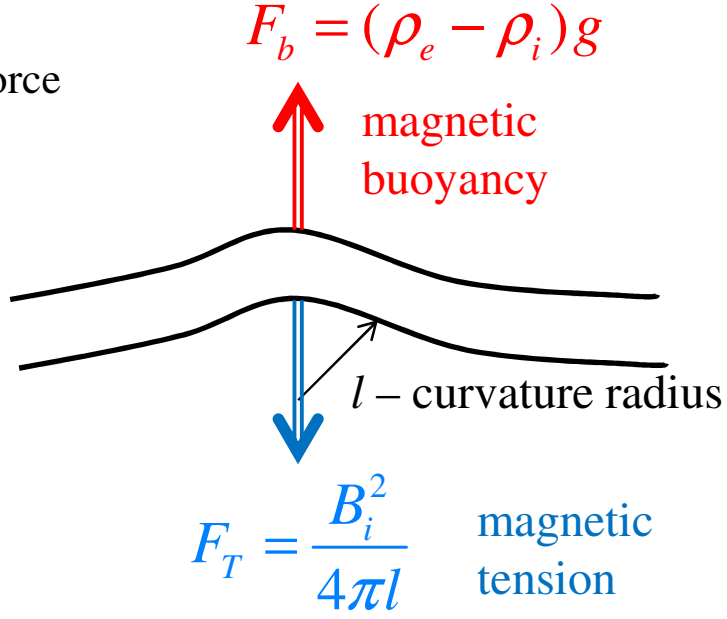

The tension force (the first term) can be estimated as: $\frac{B_i^2}{4\pi l}$,

where l is a characteristic size of a loop perturbation.

The instability condition: $(\rho_e - \rho_i)g > \frac{B_i^2}{4\pi l}$,

or using the equilibrium condition: $l > \frac{2RT}{g} = 2H_P$,

where H_P is the pressure scale height. Magnetic buoyancy is particularly strong near the surface where the pressure scale height is small because of the relatively low temperature.

Characteristic time of magnetic flux emergence

The emergence time scale: $\tau \sim \frac{d}{v_A}$,

where d is the initial depth of the tube, v_A is a characteristic Alfven speed.

For a 10,000 G tube at the base of the convection zone ($\rho = 0.2$ g/cm^3, $d = 2\times10^{10}$ cm): $v_A \sim 60$ m/s, $\tau \sim 2$ months.

If the emergence time is longer than the period of rotation then the Coriolis force affects the directions of the emergence. The tubes are deflected towards higher latitudes. The flux tubes at the bottom of the convection zone must have the field strength of about 60,000 G to emerge at mid latitudes.

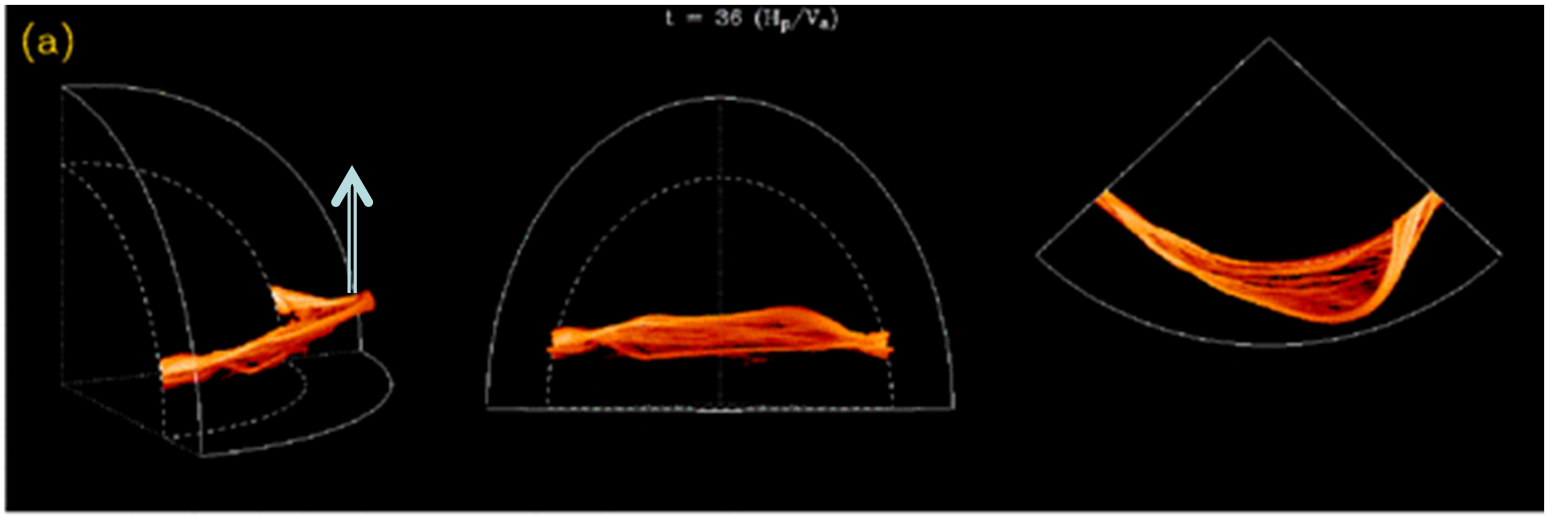

Sunspots.

Biermann (1941) first suggested that sunspots are dark because convection is suppressed by magnetic field. However, heat accumulated beneath the spot would increase pressure and disperse the magnetic field. To stop the pressure enhancement Parker suggested strong downdrafts below the spot with speed 1-2 km/s.
The downdrafts are discovered recently by helioseismology.

Classification of sunspots (Hale, 1919):

- α - a single spot connected to a plage
- β - a pair of spots of opposite polarity
- γ - a complex irregular spot
- δ - umbras of opposite polarity within the same penumbra

Flares and CME occur mostly in δ-type sunspots.

Sunspot classification is provided by SolarMonitor.org.

www.SolarMonitor.org

Date Search | 6 September 2017 | NOAA Search

⇐20170905 ⇐Week ⇐Rotation | Today | Rotation⇒ Week⇒ 20170907⇒

Main | Far-side | SDO short-wave | SDO long-wave

NOAA
6 Active Regions

Flare Forecast

Coronal Holes

HMI Mag 20170906 18:46

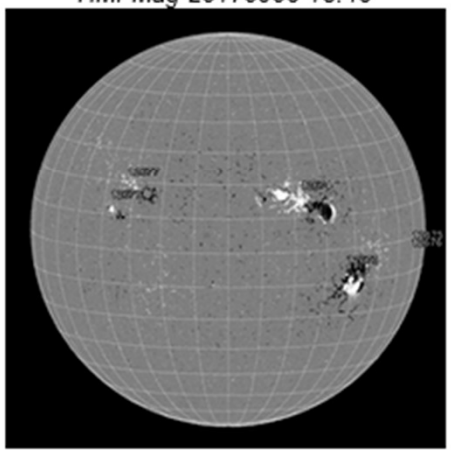

HMI 6173Å 20170906 18:46

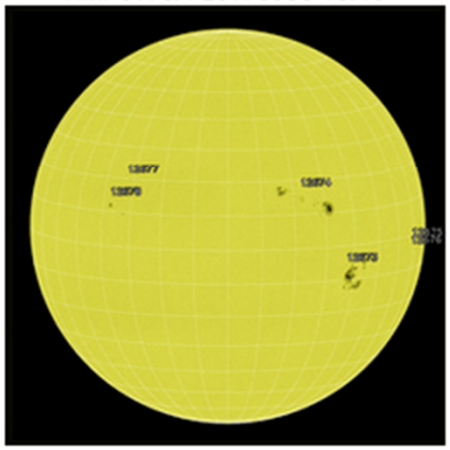

GHN Hα 20170906 08:24

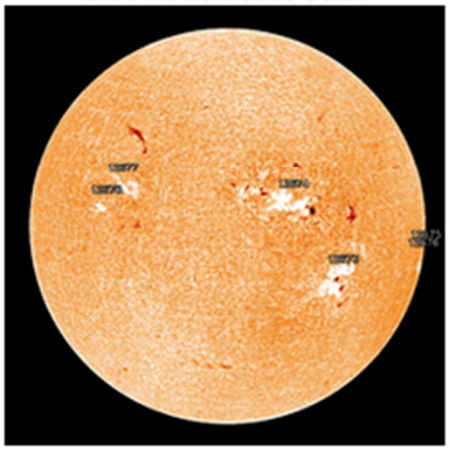

SWAP 174Å 20170906 18:34

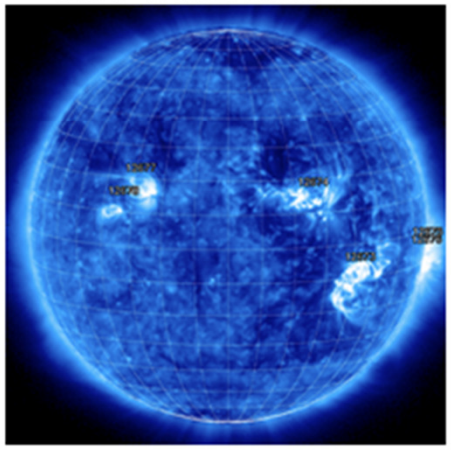

AIA 193Å 20170906 19:27

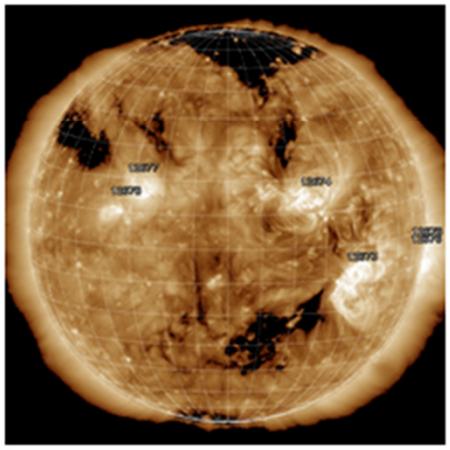

XRT 20170905 17:57

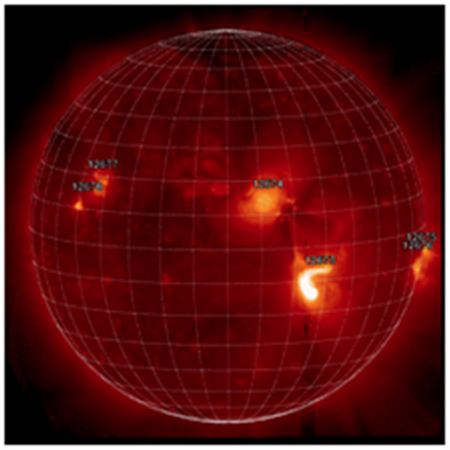

GOES
ACE
SDO/EVE
Events

LATEST Most Active Region -- NOAA 12673 -- 2 X-class, 4 M-class, and 8 C-class flares

Today's/Yesterday's NOAA Active Regions						
NOAA Number	*Latest Position*	*Hale Class*	*McIntosh Class*	*Sunspot Area [millionths]*	*Number of Spots*	*Recent Flares*
12673	S09W42 (630",-236")	βγδ/βγδ	Dkc/Dkc	0880/0680	33/28	X9.3(11:53) X2.2(08:57) C2.7(07:29) C1.5(20:00) / M2.3(17:37) C4.6(17:11) C3.7(16:14) C6.9(13:26) C2.2(12:30) C5.4(10:13) M3.2(04:33) M1.0(03:42) M4.2(01:03) C9.8(00:30)
12674	N14W26 (406",124")	β/β	Fhi/Fhi	0680/0740	23/34	-
12675	S07W91 (944",-112")	β/β	Bxo/Bxo	0010/0010	01/04	-
12676	S09W88 (939",-151")	β/β	Bxo/Cro	0030/0030	02/04	-
12677	N18E28 (-426",191")	α/α	Axx/Axx	0020/0010	01/02	-
12678	N11E33 (-510",81")	β/-	Bxo/---	0010/----	02/--	C1.6(06:17) / -

Class (HH:MM) -Today
Class (HH:MM) -Yesterday

www.SolarMonitor.org

Date Search

6 September 2017

NOAA Search

⇐20170905 ⇐Week ⇐Rotation

Today

Rotation⇒ Week⇒ 20170907⇒

Main | Far-side | SDO short-wave | SDO long-wave

NOAA
6 Active Regions

Flare Forecast

Coronal Holes

HMI Mag 20170906 18:46

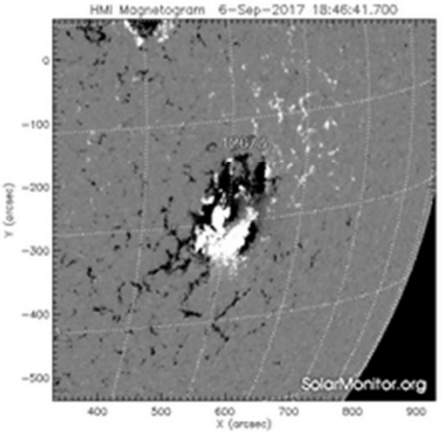

HMI 6173Å 20170906 18:46

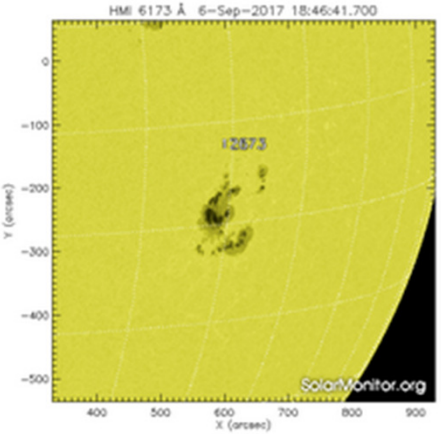

GHN Hα 20170906 08:24

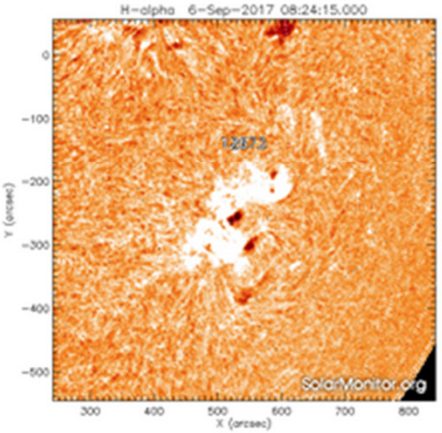

SWAP 174Å 20170906 18:34

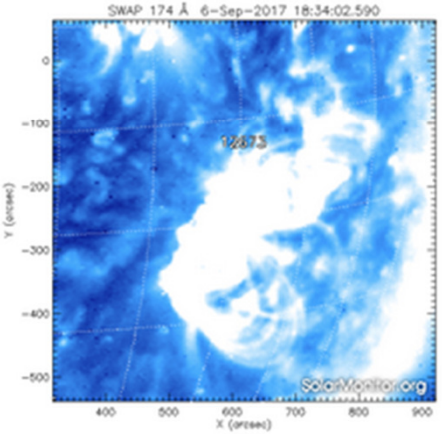

AIA 193Å 20170906 19:27

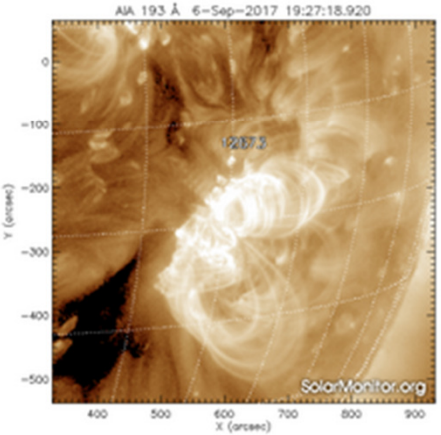

XRT 20170905 17:57

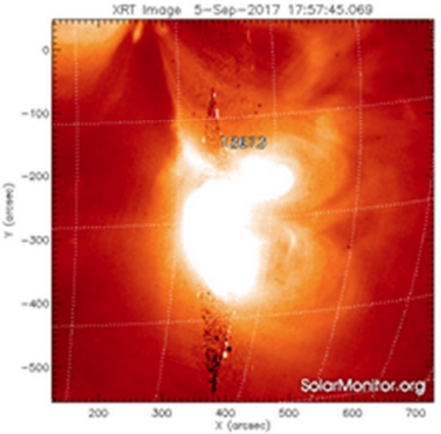

GOES
ACE
SDO/EVE
Events

LATEST Most Active Region -- NOAA 12673 -- 2 X-class, 4 M-class, and 8 C-class flares

Example of βγδ sunspot group: AR 12673, Sept. 6, 2017

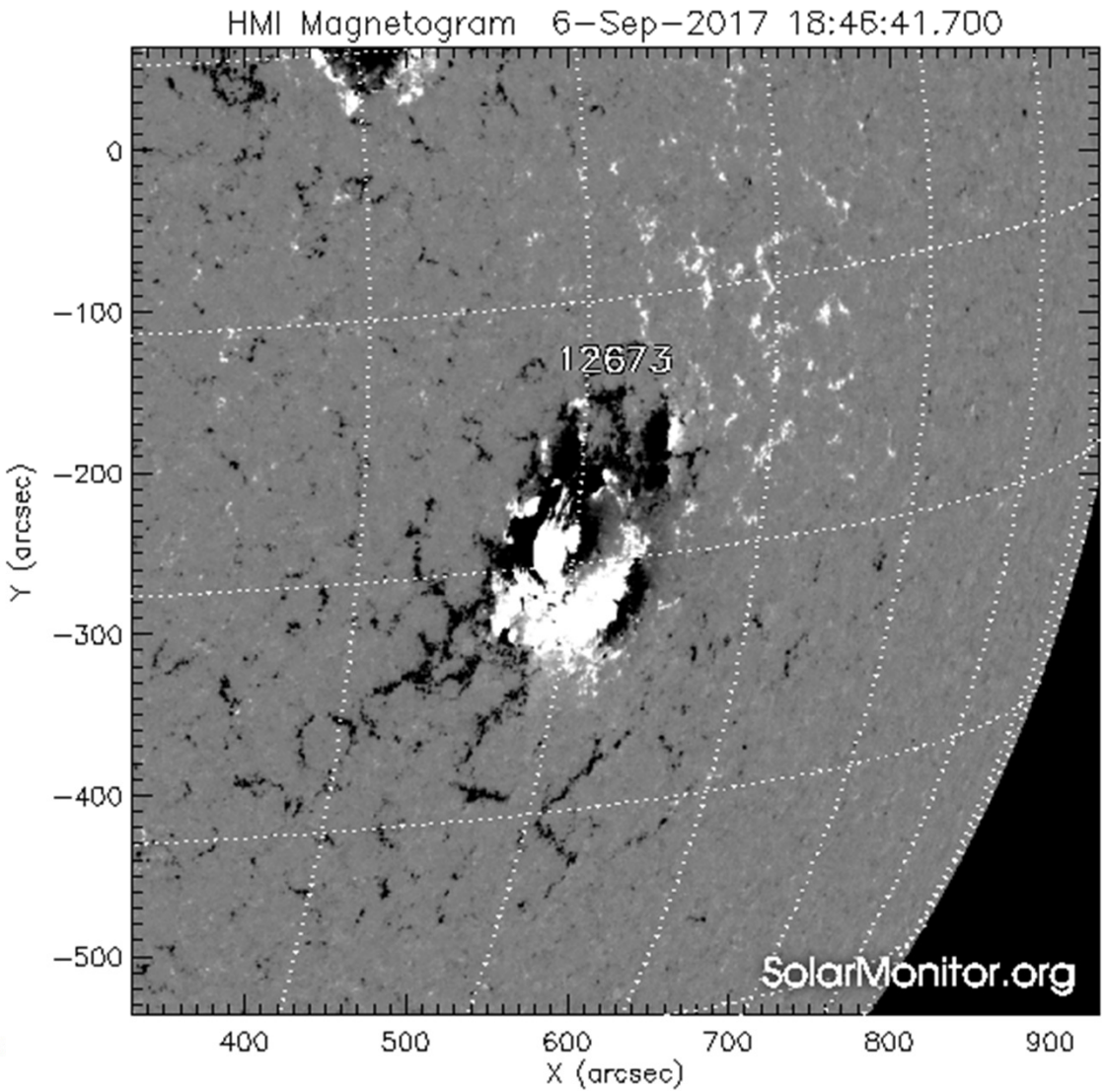

α - a single spot conne

β - a pair of spots of opposite polarity

γ - a complex irregular spot

δ - umbras of opposite polarity within the same penumbra

Example of βγδ sunspot group: AR 12673, Sept. 6, 2017

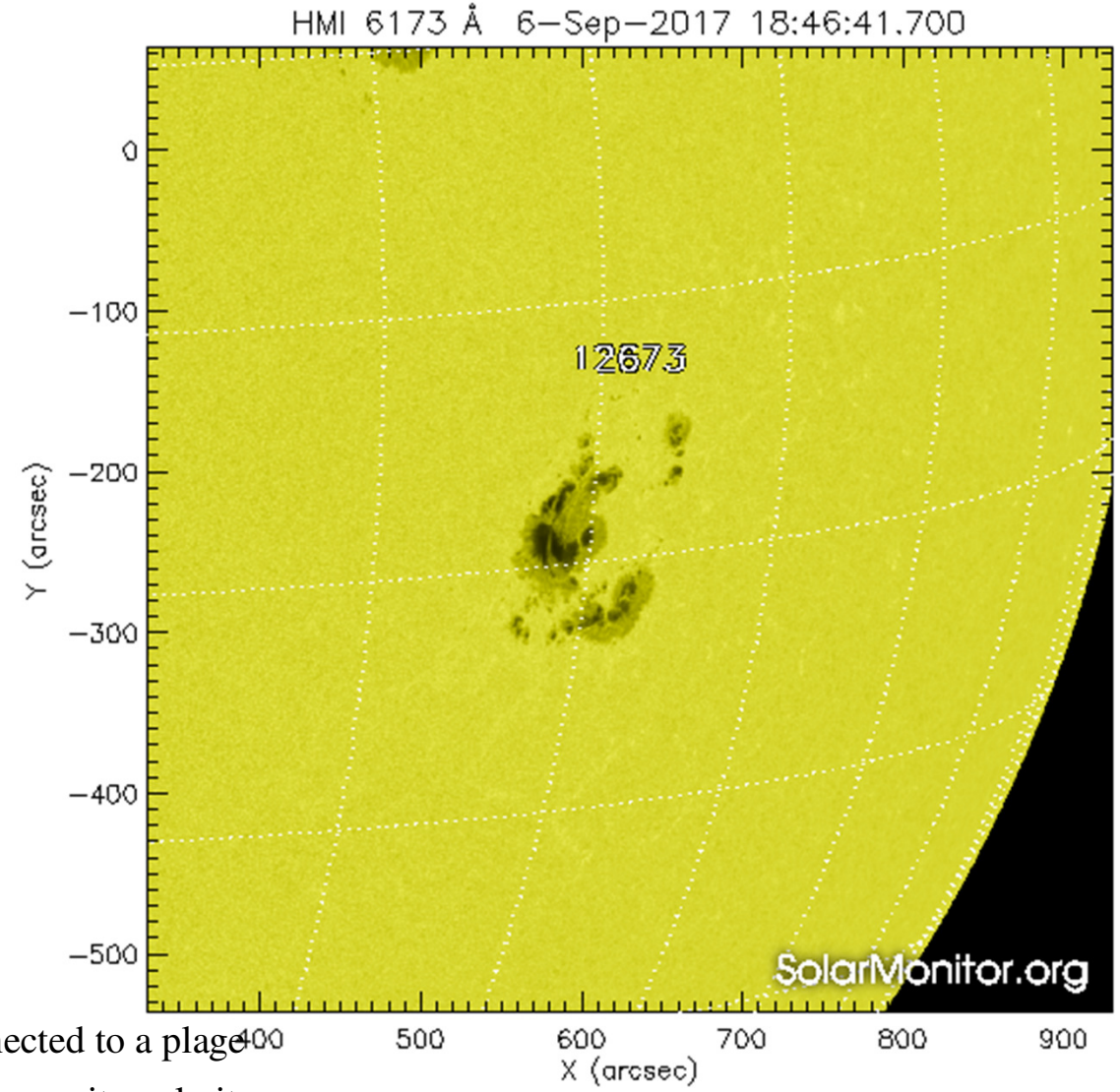

α - a single spot connected to a plage

β - a pair of spots of opposite polarity

γ - a complex irregular spot

δ - umbras of opposite polarity within the same penumbra

Small magnetic elements

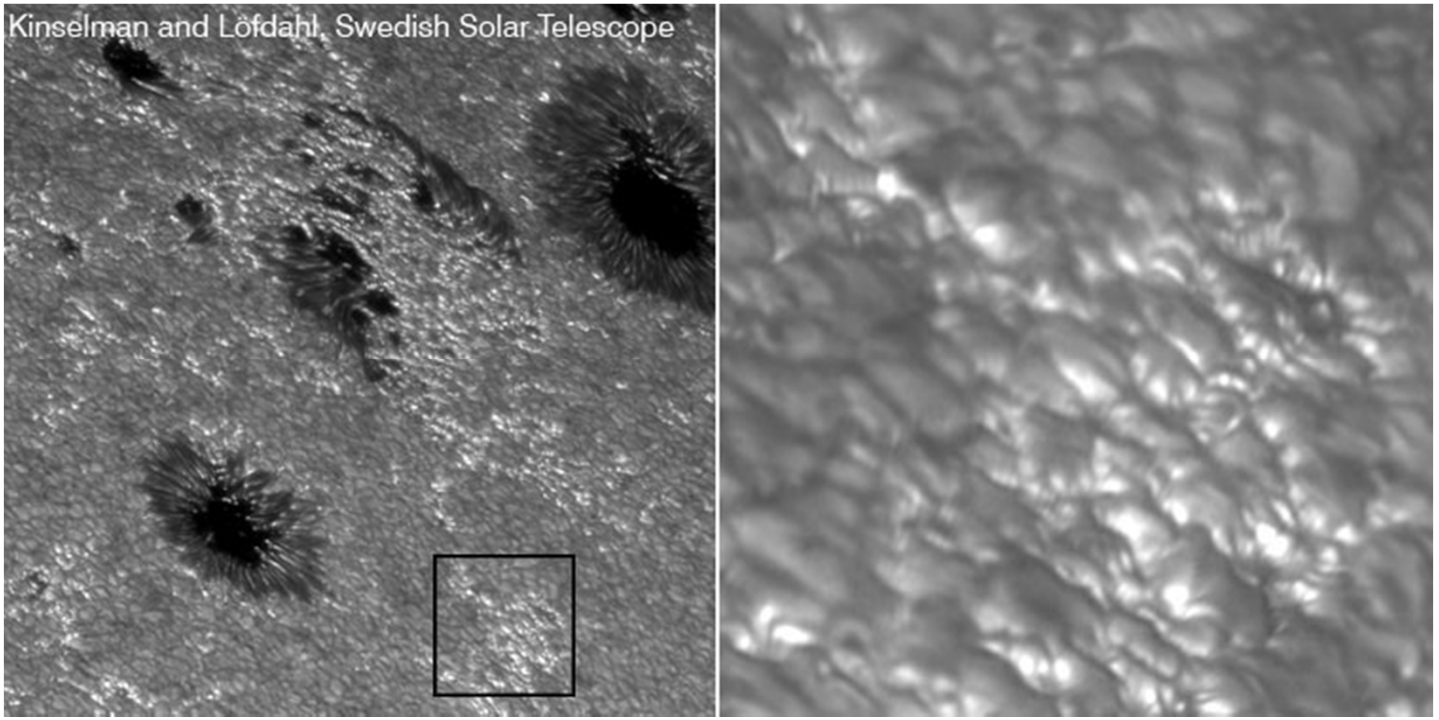

Small magnetic elements that constitute plages are brighter near the limb because we see "hot wall" in deeper layers (since density inside the flux tubes is lower the layer of optical depth 1.

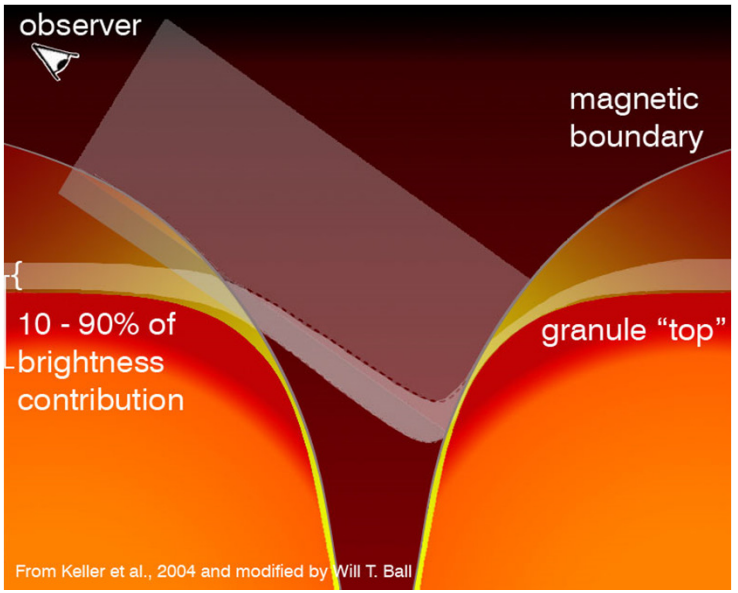

Monolithic and cluster models of sunspots

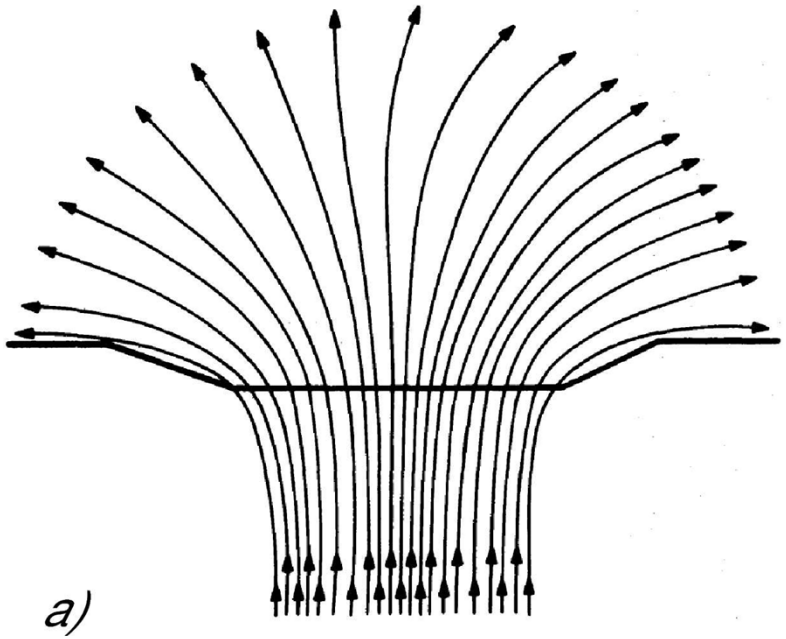

Monolithic model: magnetic field is confined by the gas pressure below the surface. This model is hydrostatic.

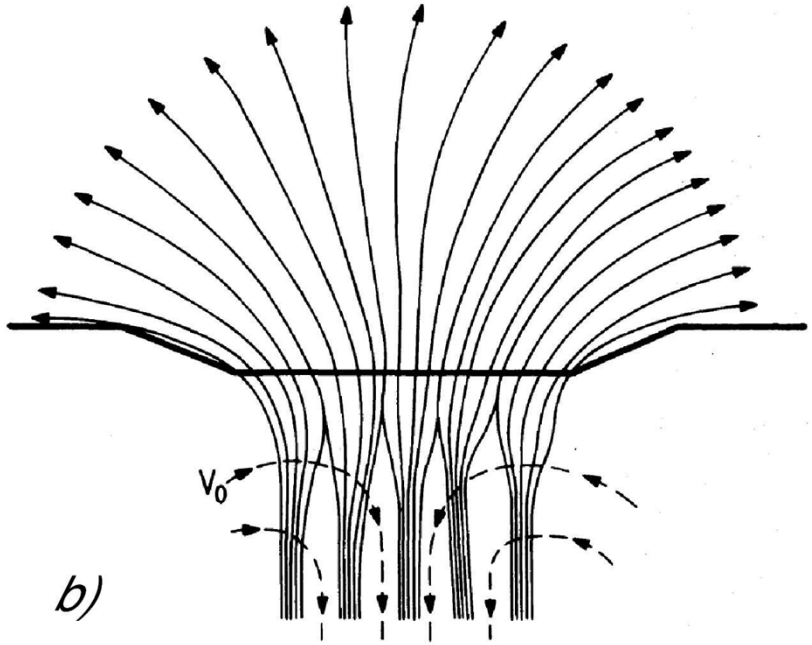

Cluster model: the sunspot magnetic structure represents a cluster of magnetic flux tubes hold together by converging downdrafts below the surface.

Numerical MHD models of sunspot formation

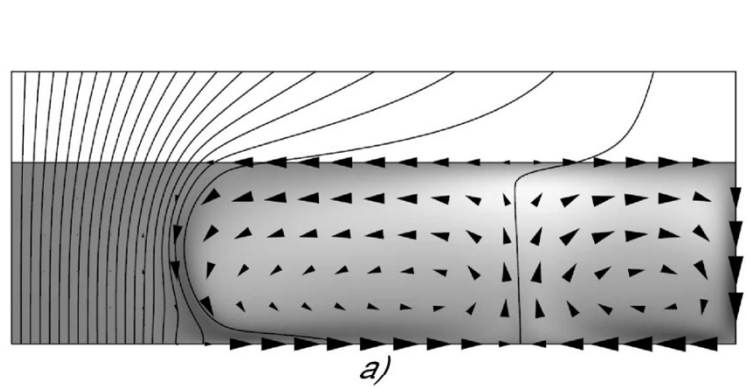

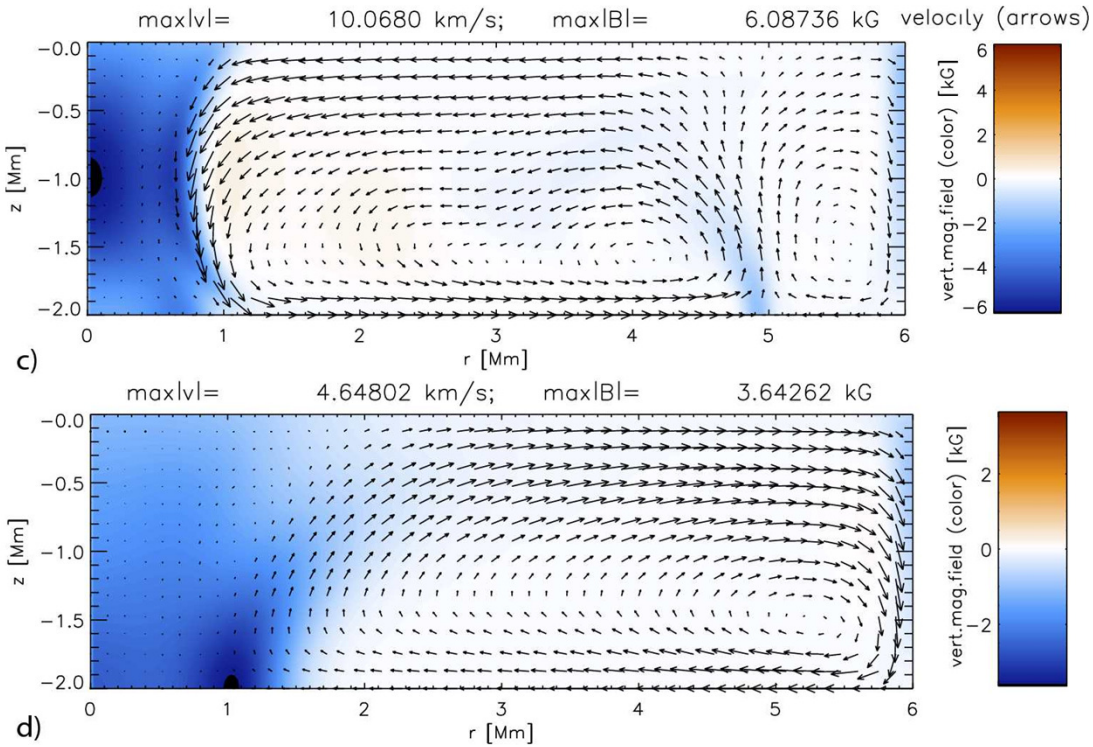

Numerical MHD models of the formation of magnetic structures in a convective layer concluded that stable magnetic structures can be formed only by converging flows, and diverging flows inevitably tore the structures apart. They suggested that the Evershed and moat flows are confined in a near-surface layer, and that beneath these there is a converging “collar” flow that provides the stability of sunspots (Hurlburt et al, 2000)

Imaging of the sunspot subsurface structure and flows by time-distance helioseismology

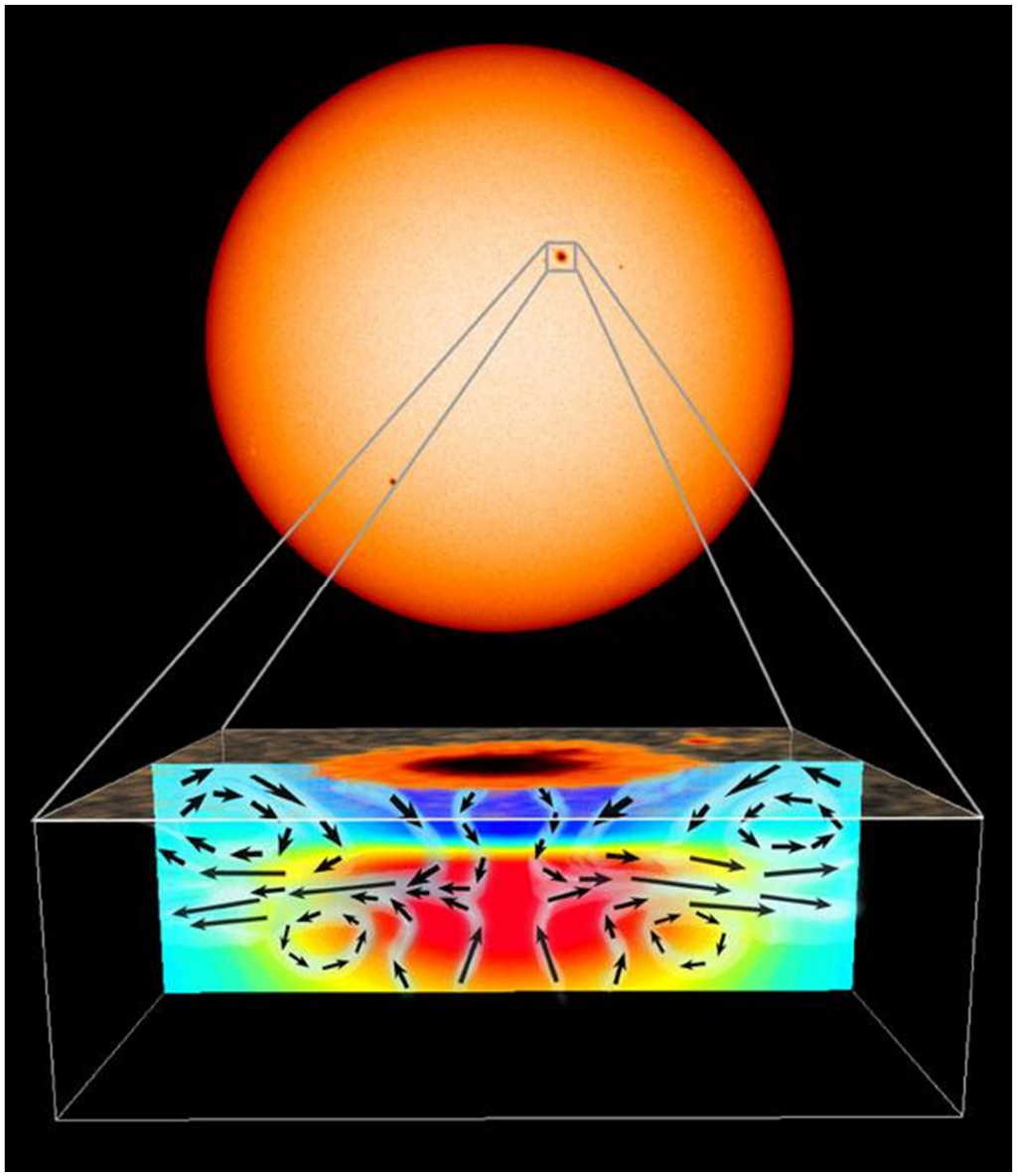

The intense magnetic field below a sunspot strangles the normal up-flow of energy from the hot solar interior, leaving the spot cooler and therefore darker than its surroundings (dark blue region in the cross-section image). The suppression of the bubbling convective motions forms a kind of plug that prevents some of the energy in the interior from reaching the surface. As a result, the material above the plug cools and becomes denser, causing it to plunge downward at up to 1 km/s.

That draws the surrounding plasma and magnetic field inward toward the sunspot's center. The concentrated field promotes further cooling, and as that cooling plasma sinks it draws in still more plasma, thereby setting up a self-perpetuating cycle. These plasma flows are represented by the black arrows near the top of the cross-section image, in and around the cool, dark blue region. As long as the magnetic field remains strong, the cooling effect will maintain an inflow that keeps the sunspot stable. Since the magnetic plug prevents heat from reaching the solar surface, the regions beneath the plug become hotter, which is represented by the red area beneath the blue region in the cross section image. The cool downward flows dissipate at the same depth where the hot upward flows diverge, as shown by black arrows in and around the red area.

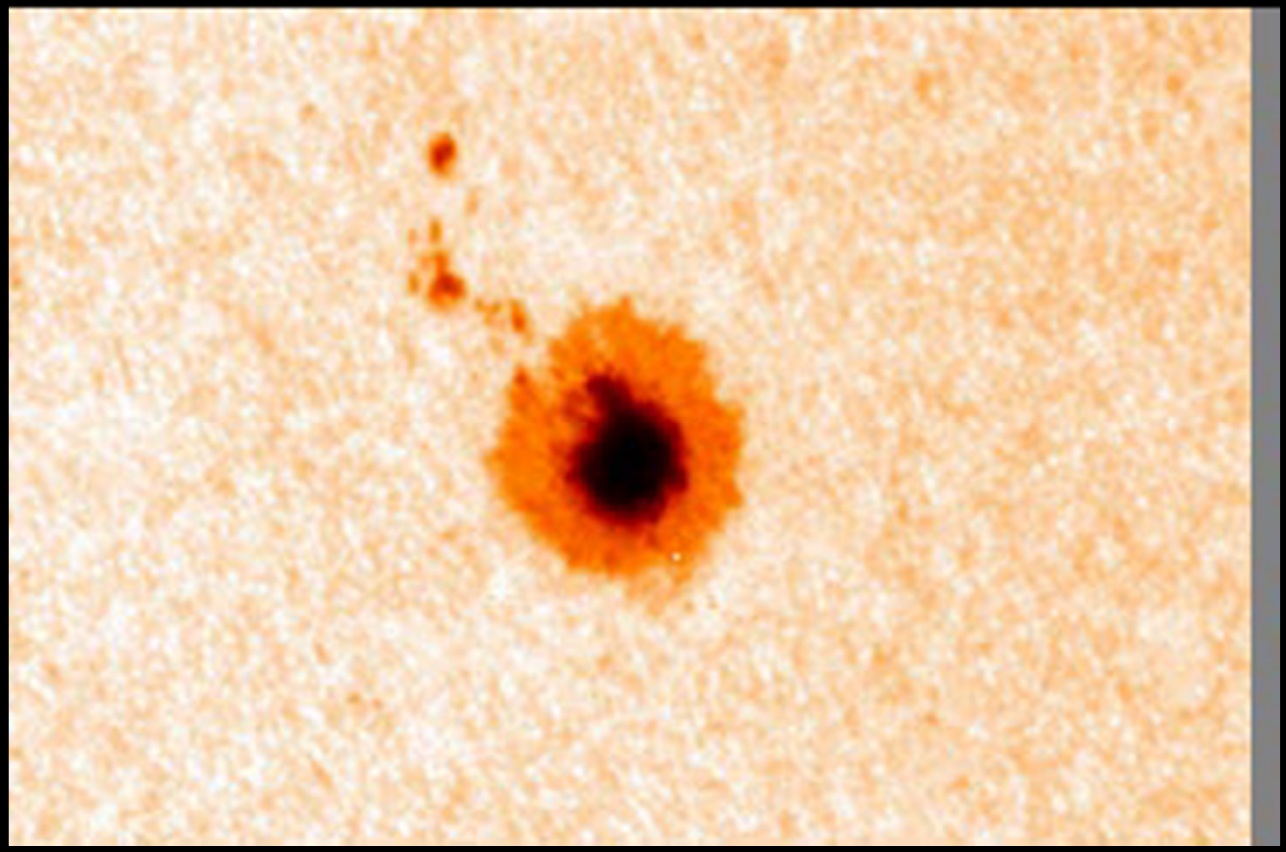

Intensity movie: notice the moat flow outside penumbra

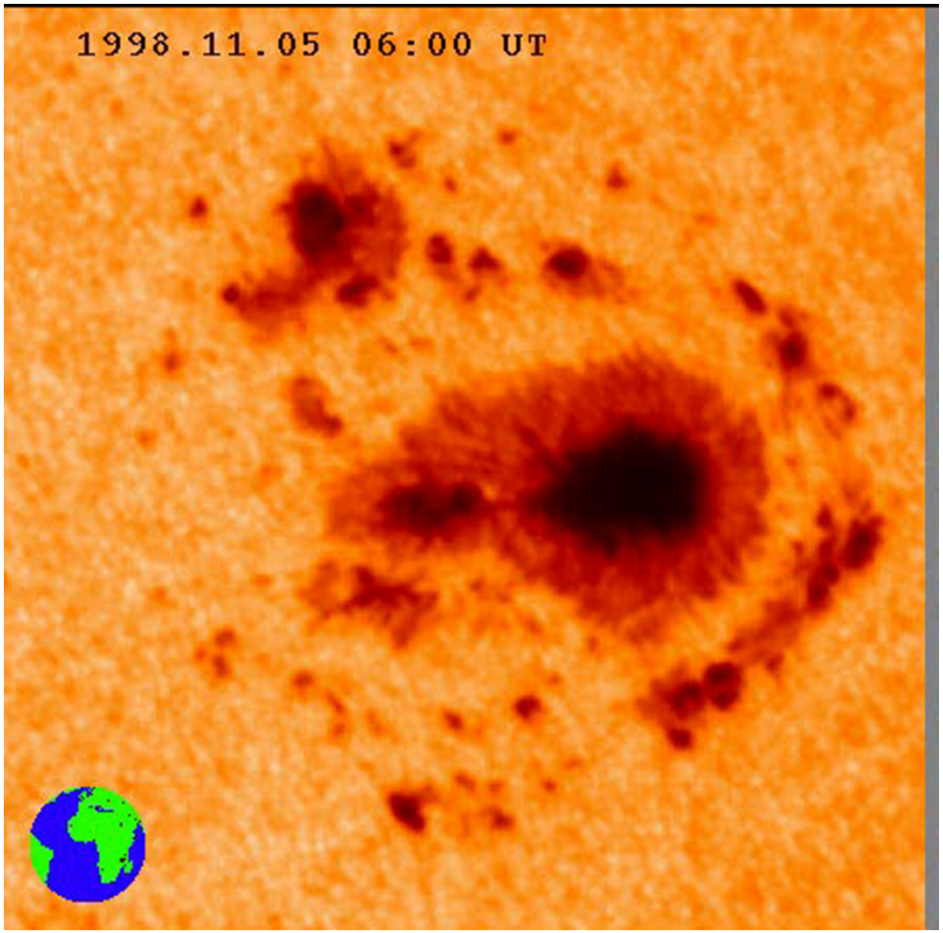

Magnetic field movie

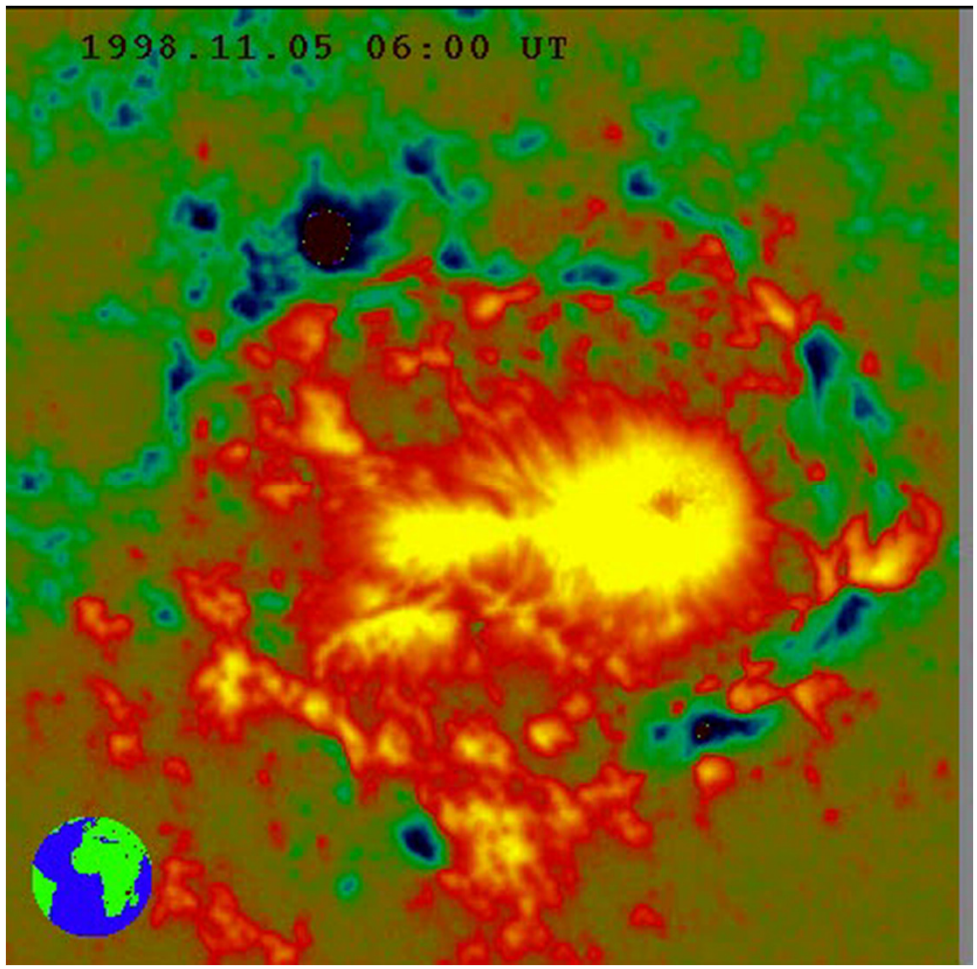

Movie of Dopplergrams shows the Evershed effect (outflow in the penumra, and the moat flow outside)

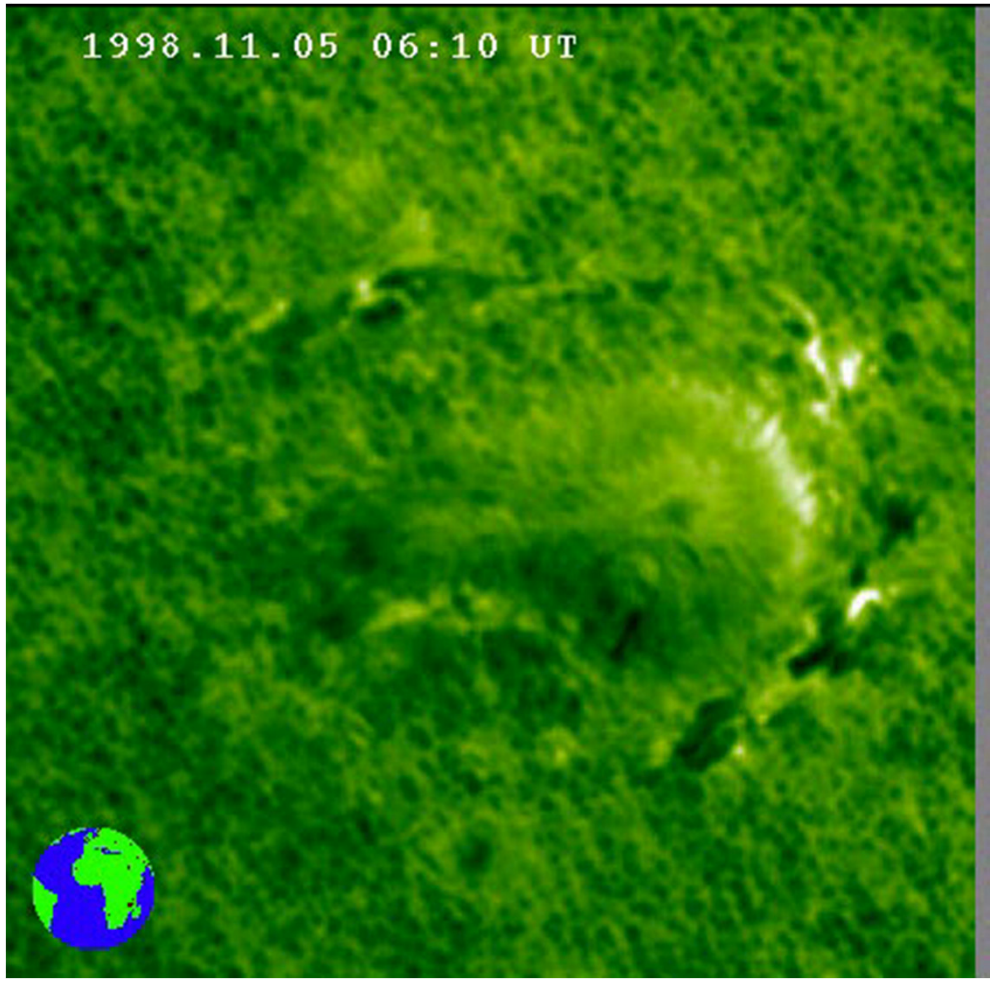

Evershed effect: outflows in penumbra filaments

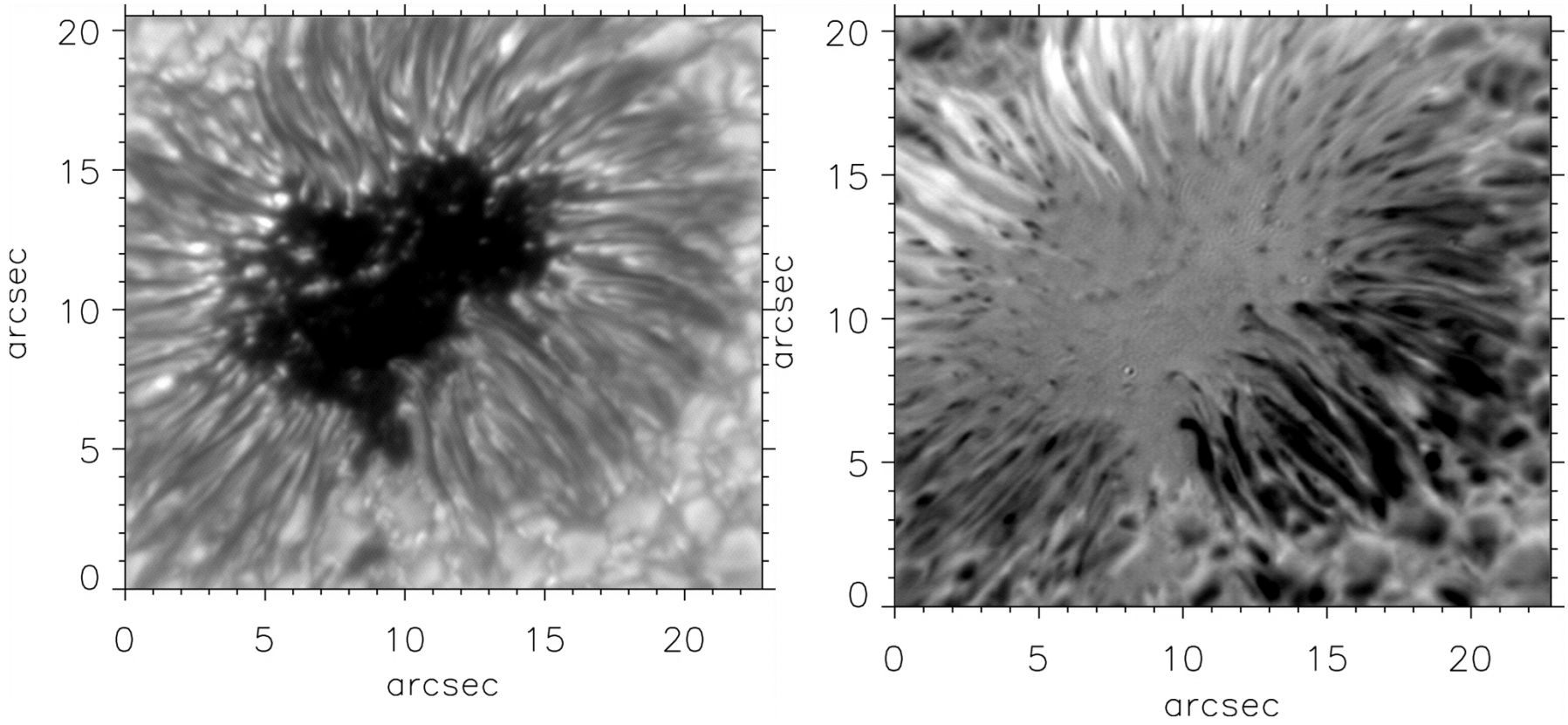

Narrowband filtergram and Dopplergram of a sunspot observed at approximately 30° away from disk center. The effective exposure time was 2.4 s. The Dopplergram shows the signature of the Evershed flow. The solar limb is toward the top left corner of these images. The velocities are encoded in a gray scale. Bright: redshift; dark: blueshift. (Rimmele, 2006)

Moving magnetic tube model

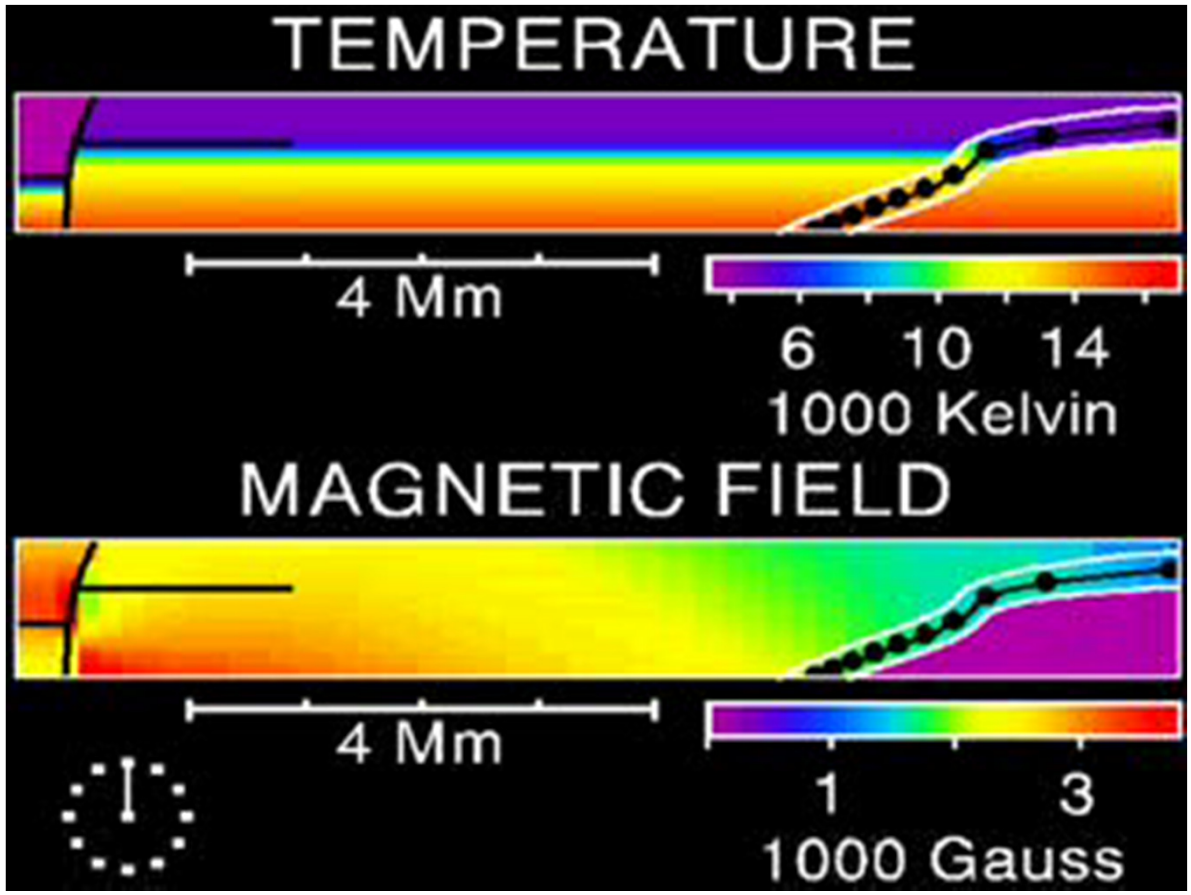

Schlichenmaier et al. (1998) model the dynamic evolution of a thin flux tube inside the penumbra. A flux tube initially located at the magnetopause becomes buoyant due to radiative heating and rises. Radiative cooling at the photosphere produces pressure differences along the loop, driving an outward-directed flow along the flux tube as it rises through the penumbra.

Moving magnetic tube model

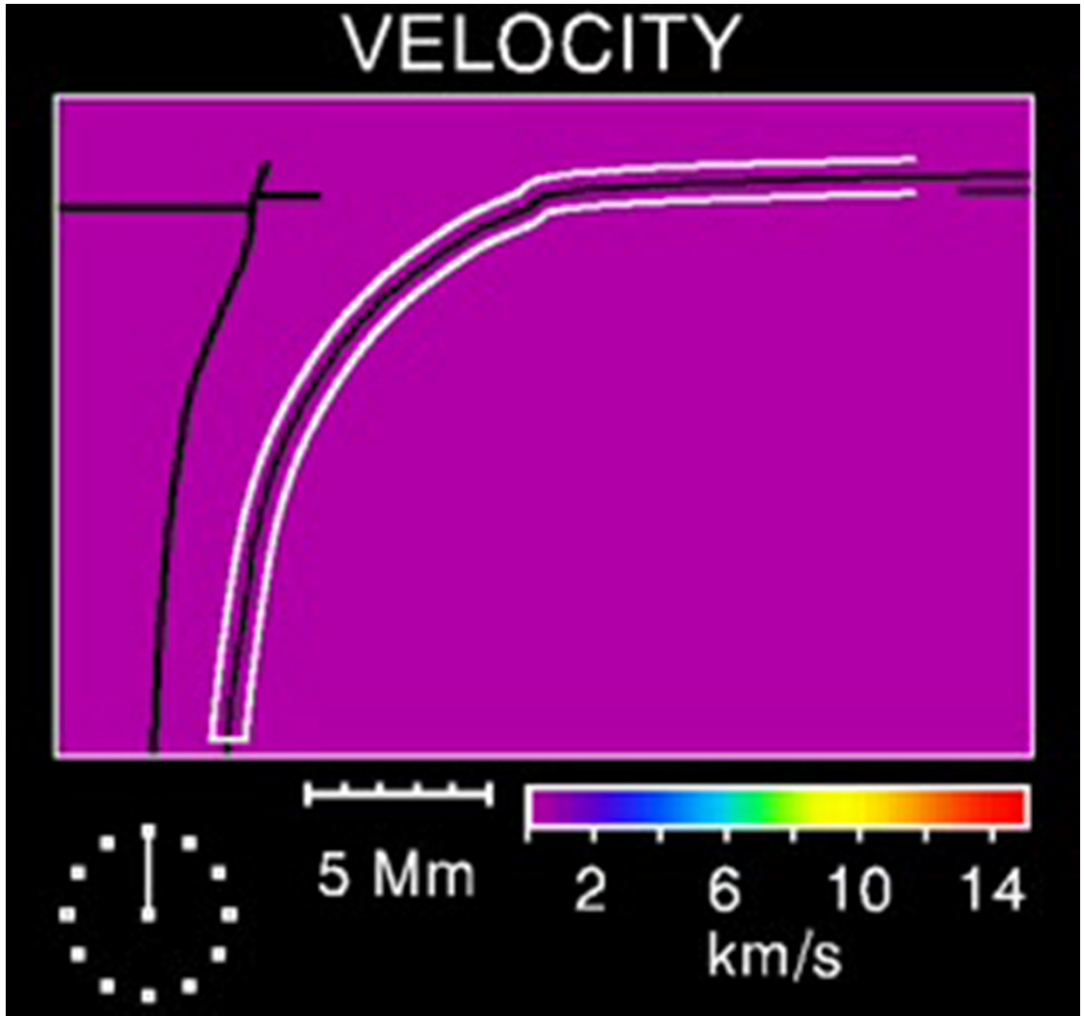

High-resolution observations of sunspots

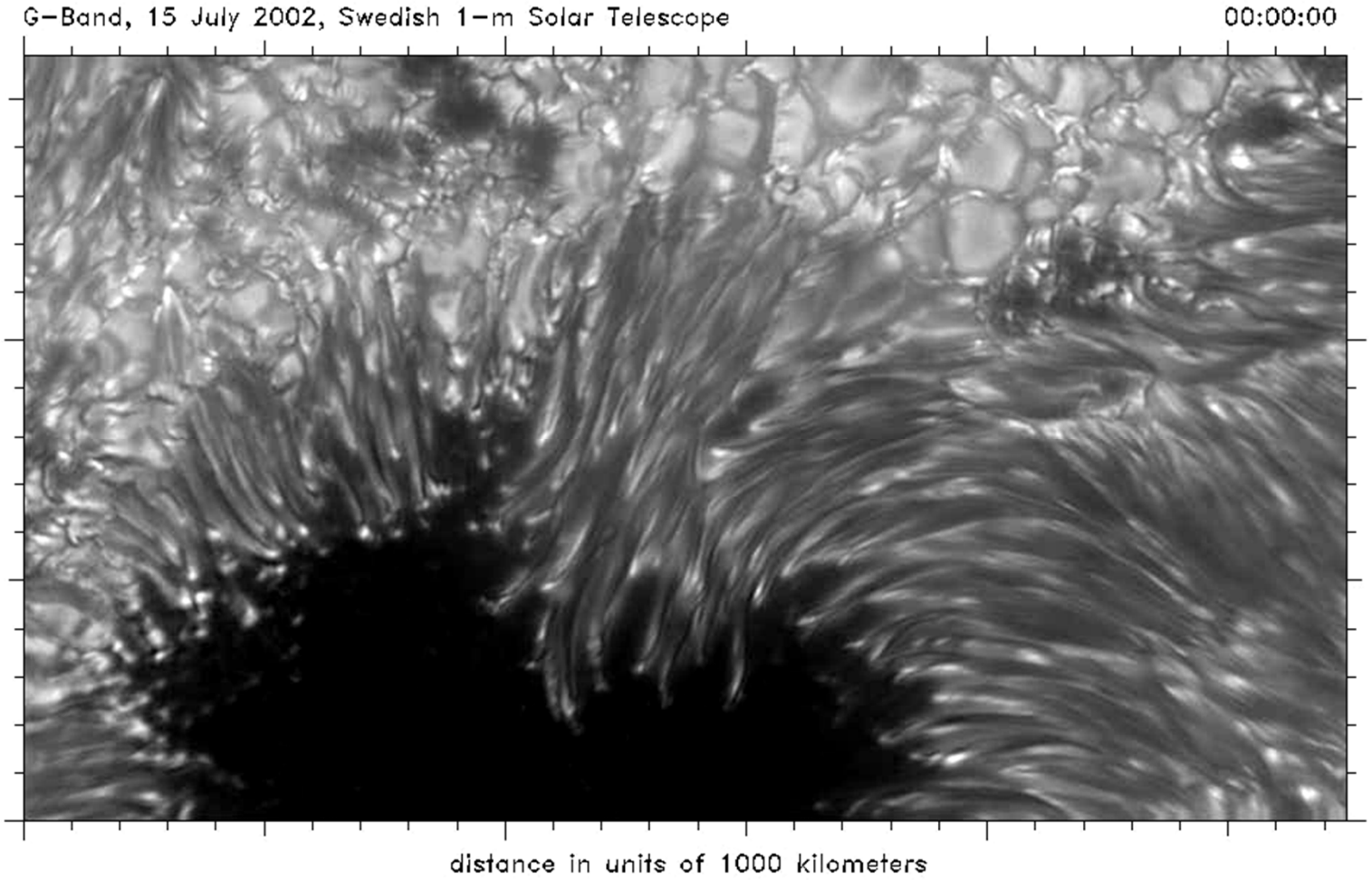

High-resolution observations of sunspots revealed complicated non-stationary twisting flow patterns in the sunspot penumbra (Scharmer et al, 2002).

It is particularly puzzling that the direction of the twisting flows is always towards the observer.

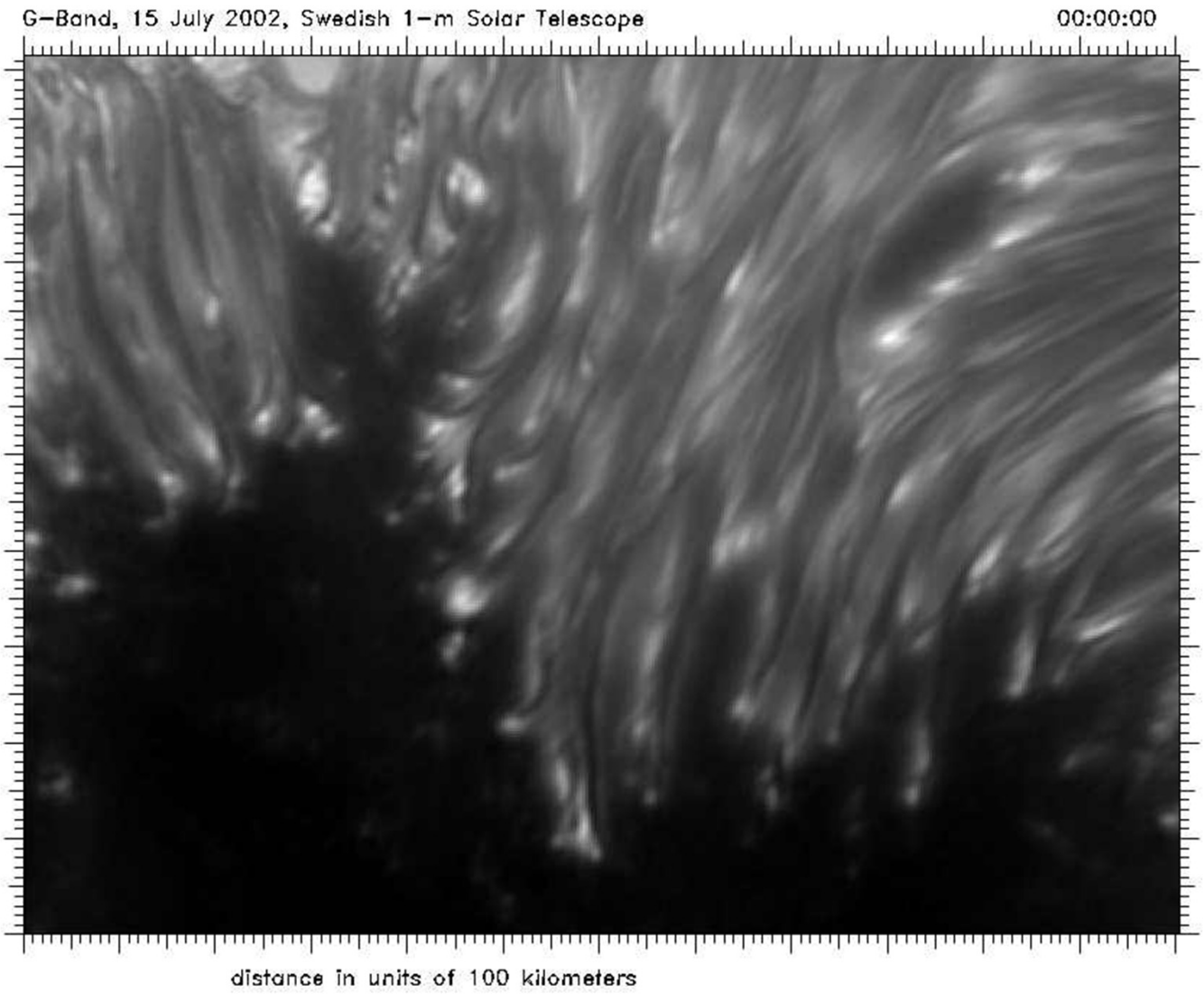
G-Band, 15 July 2002, Swedish 1-m Solar Telescope
00:00:00
distance in units of 100 kilometers

Model of Eversheds flows

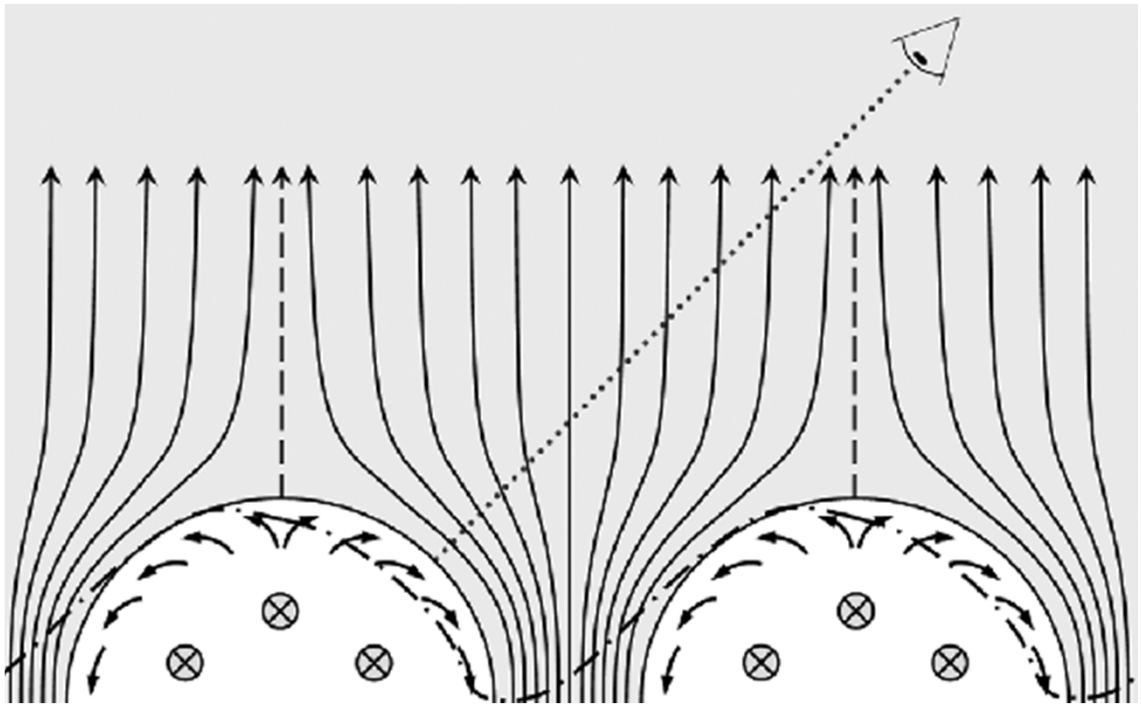

Evershed flow represent overturning convective rolls. The observer mostly see the flows rotating towards to him/her. (Spruit & Scharmer 2006)

Formation of sunspots AR 11726 (intensity)

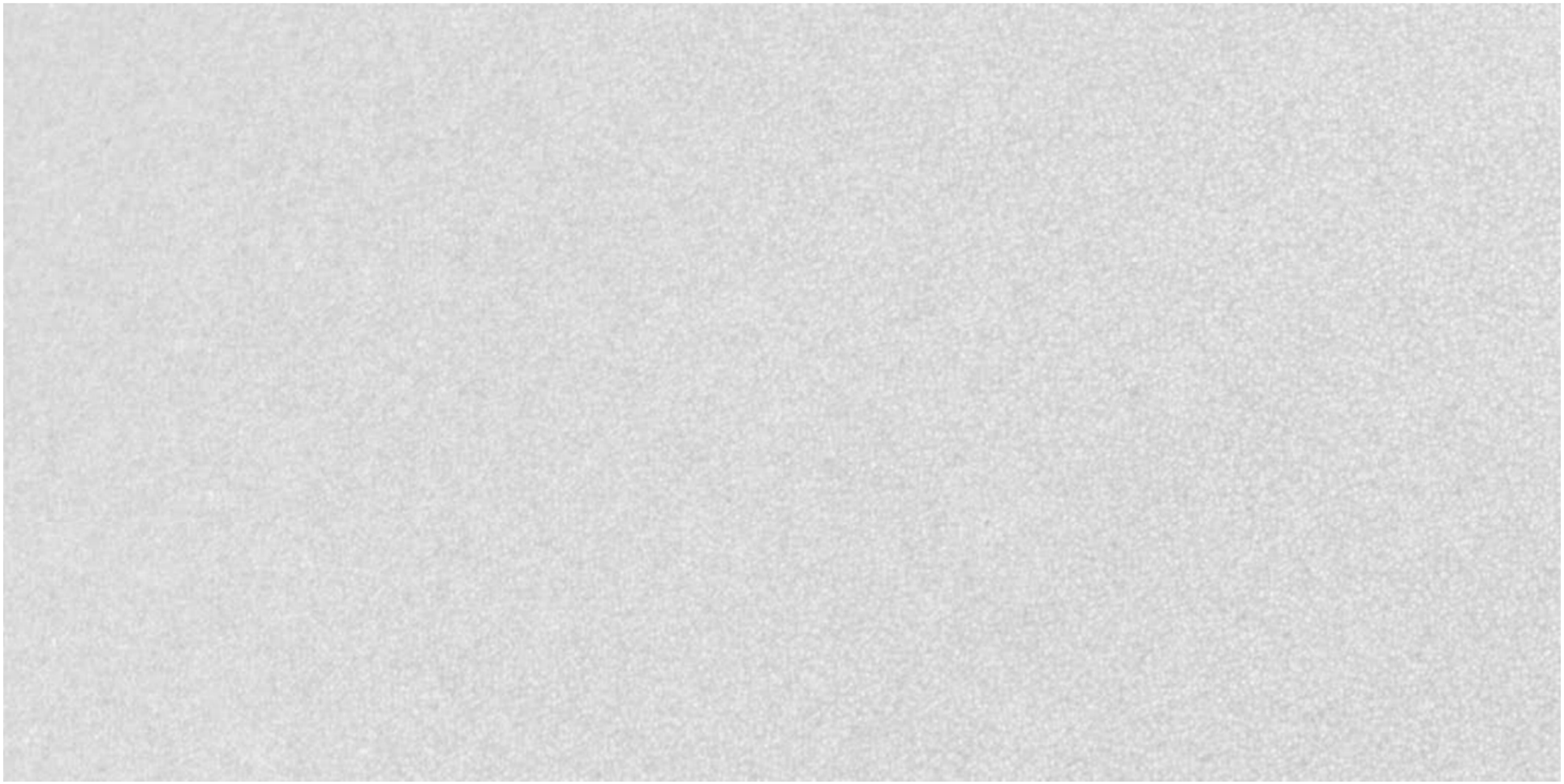

Simulations show that pore-like magnetic structures can be formed due the interaction twisting downflows (Kitiashvili 2011)

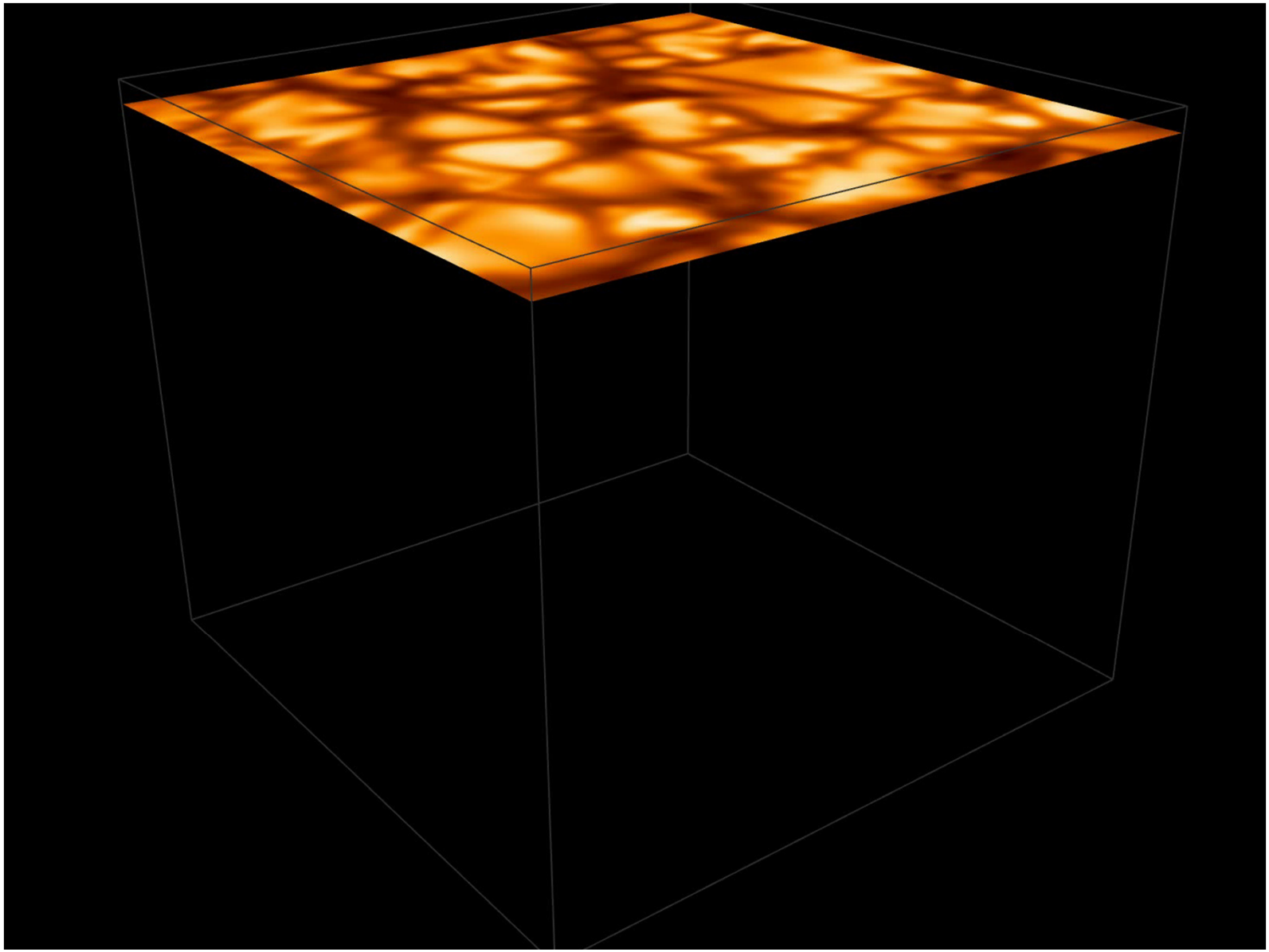

Compare with the surface dynamics of a solar pore

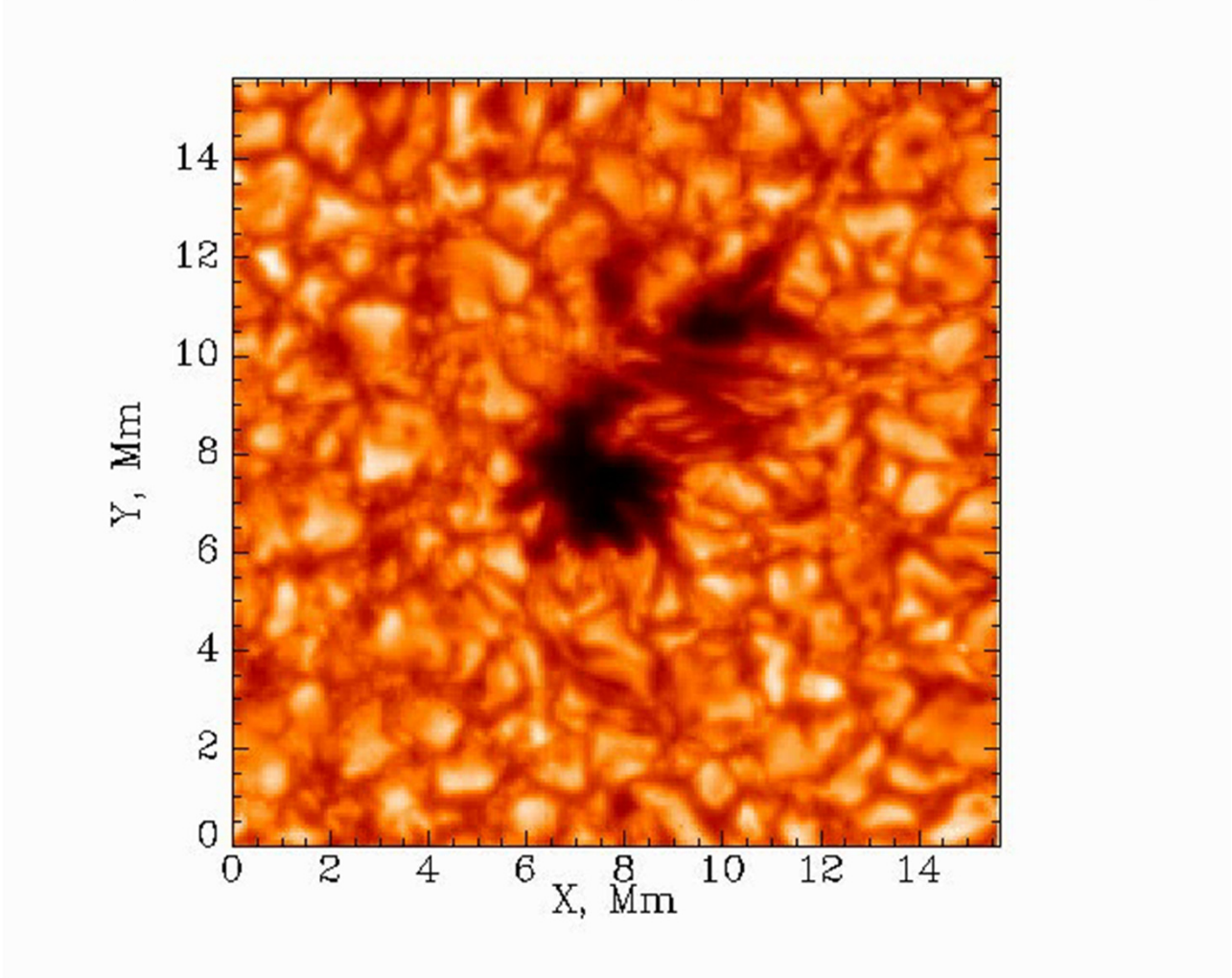

MHD Simulations of sunspots (M. Rempel)

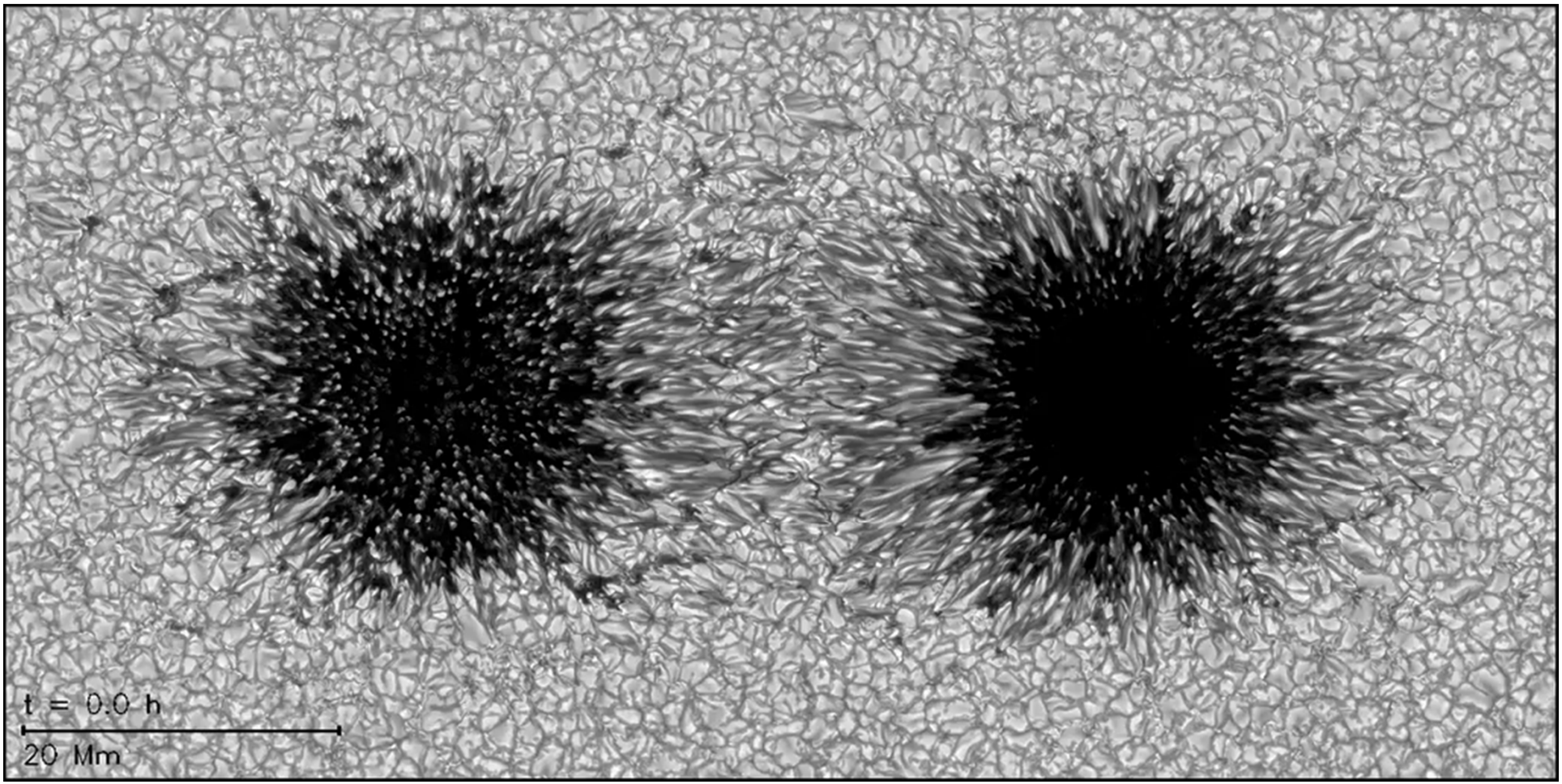

MHD Simulations of sunspots (M. Rempel)

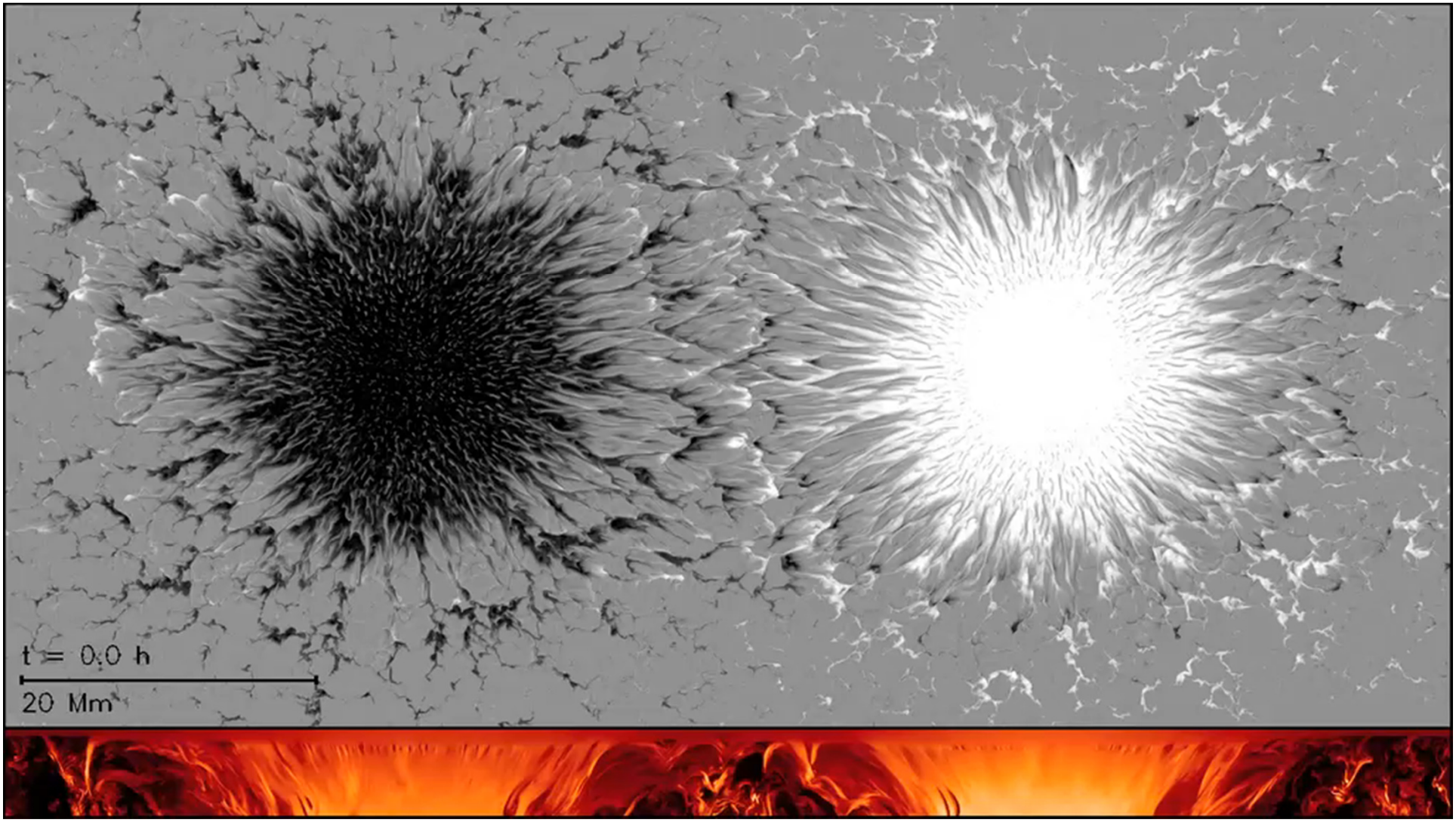

AR
11850
BBSO
TiO

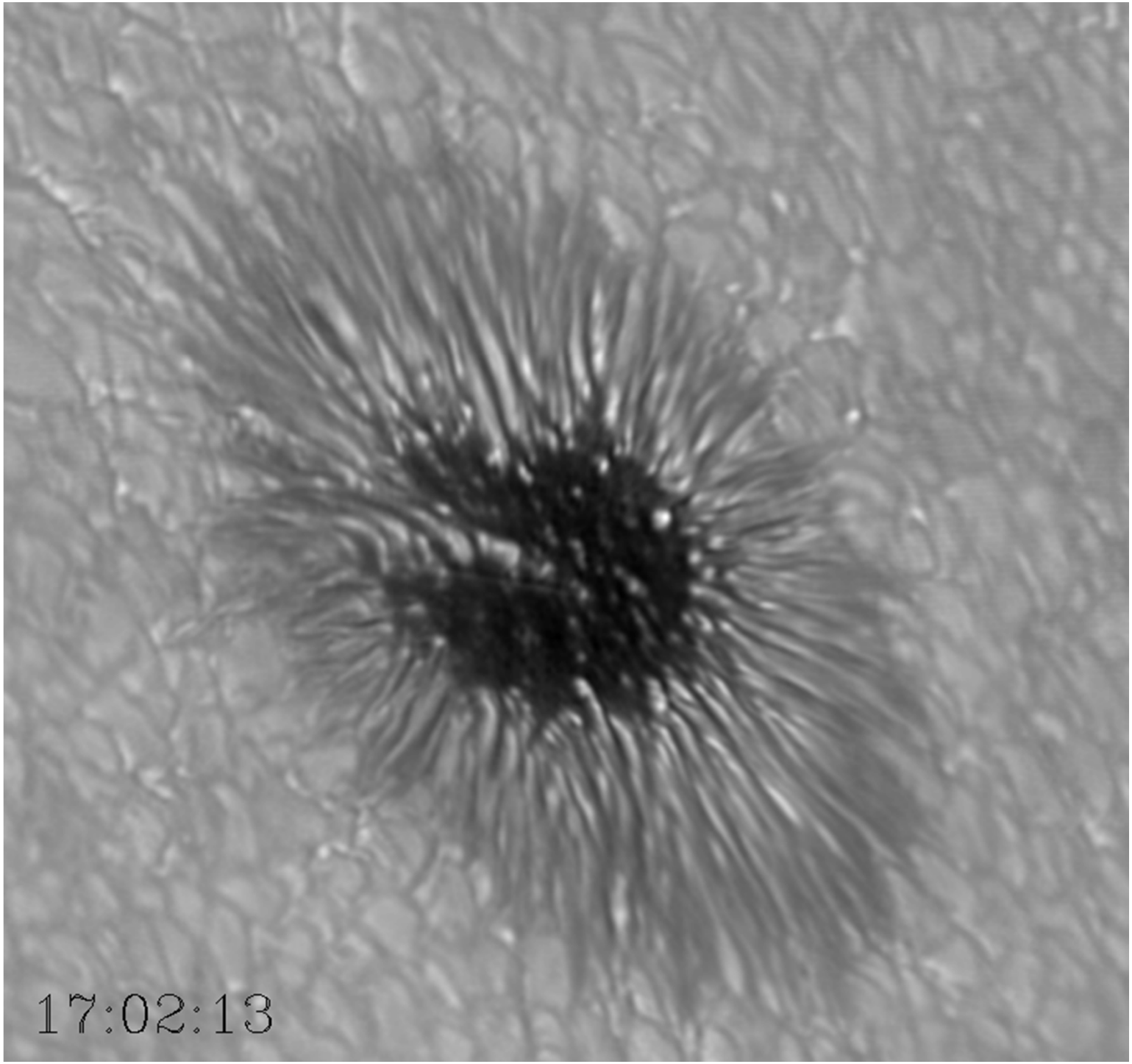

AR
11850
BBSO
Hα

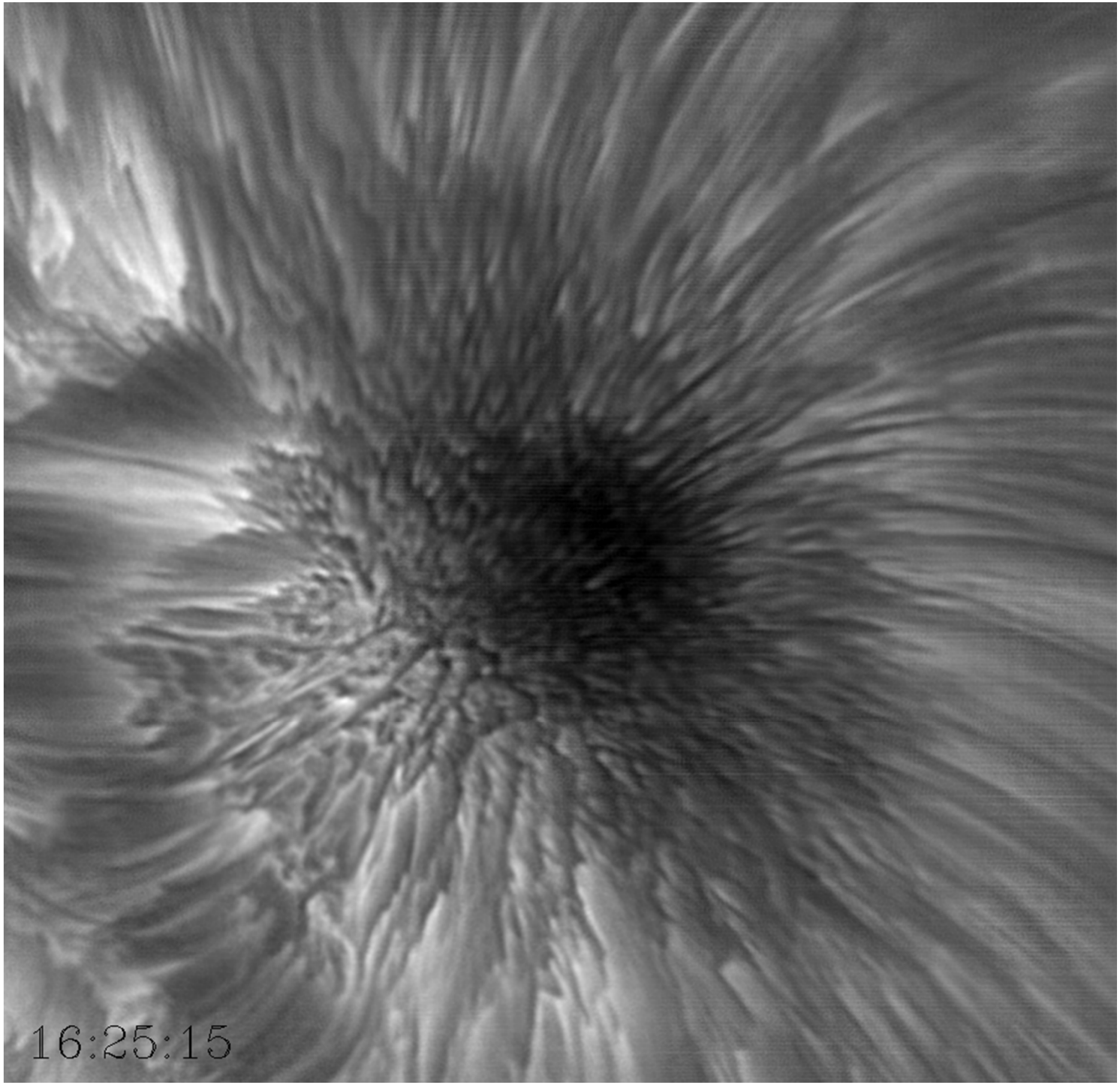

AR
11850
BBSO
Hα–0.4

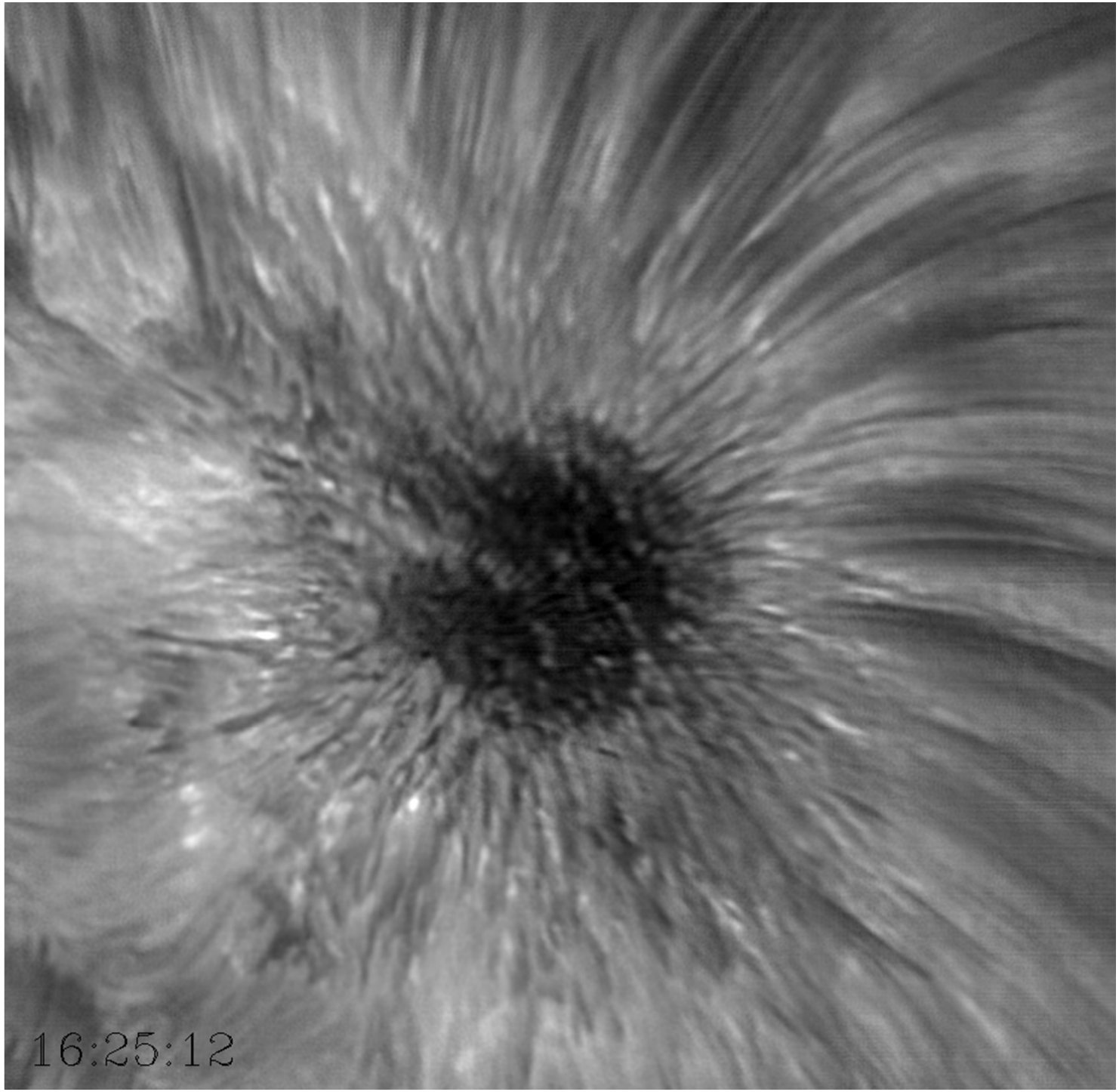

AR
11850
BBSO
Hα+0.4

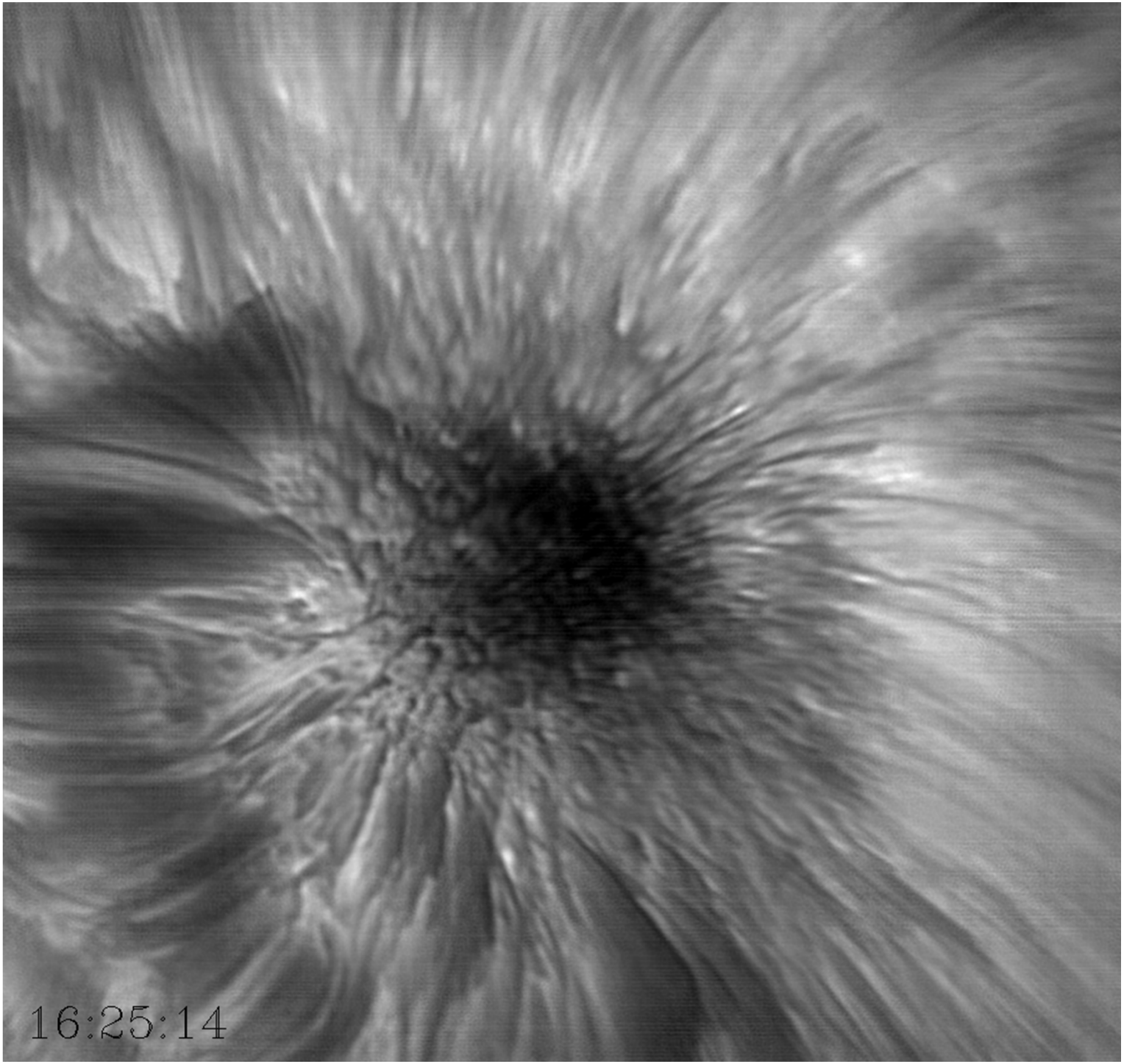

AR
11850
BBSO
Hα–0.8

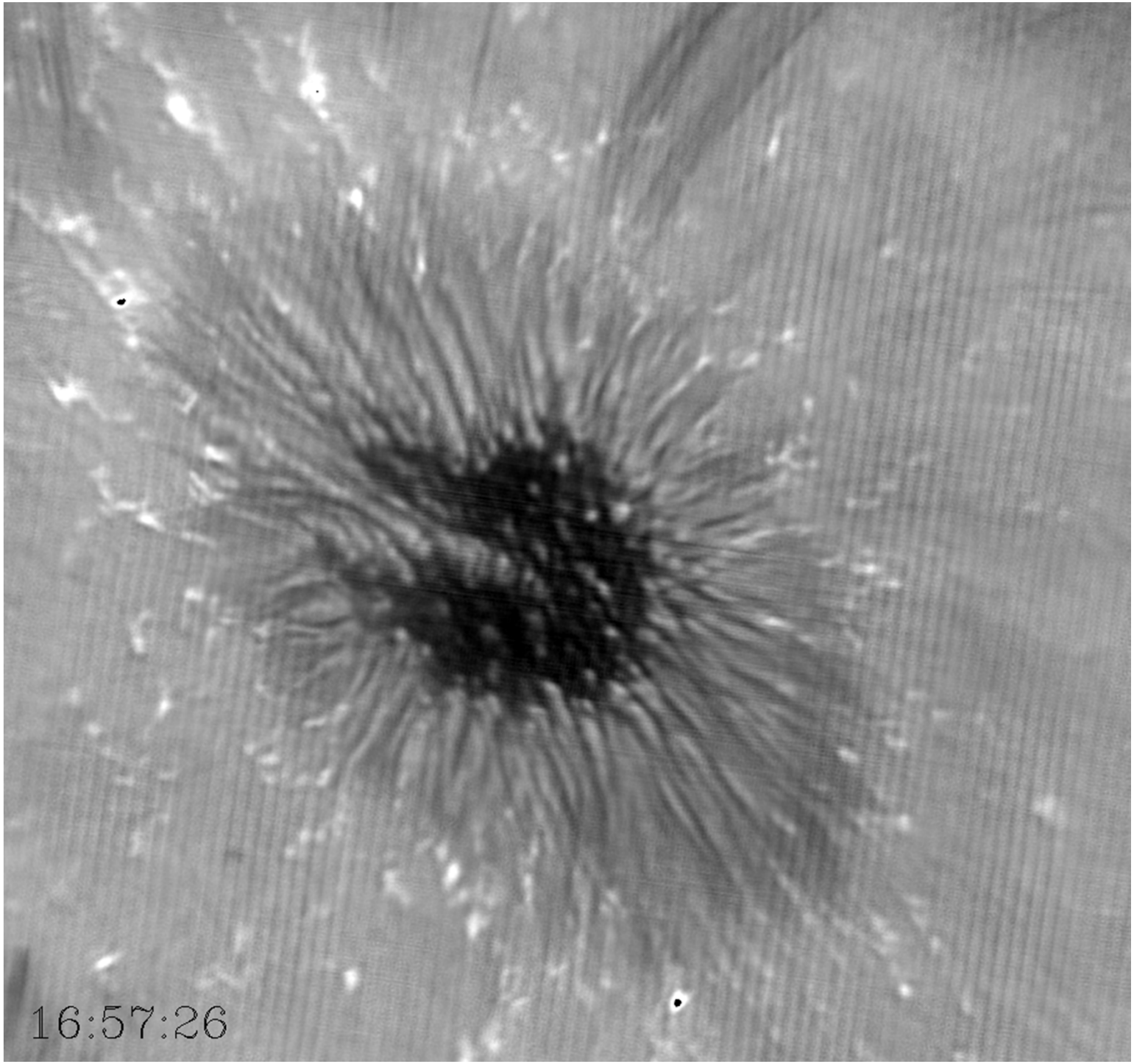

AR
11850
BBSO
Hα+0.8

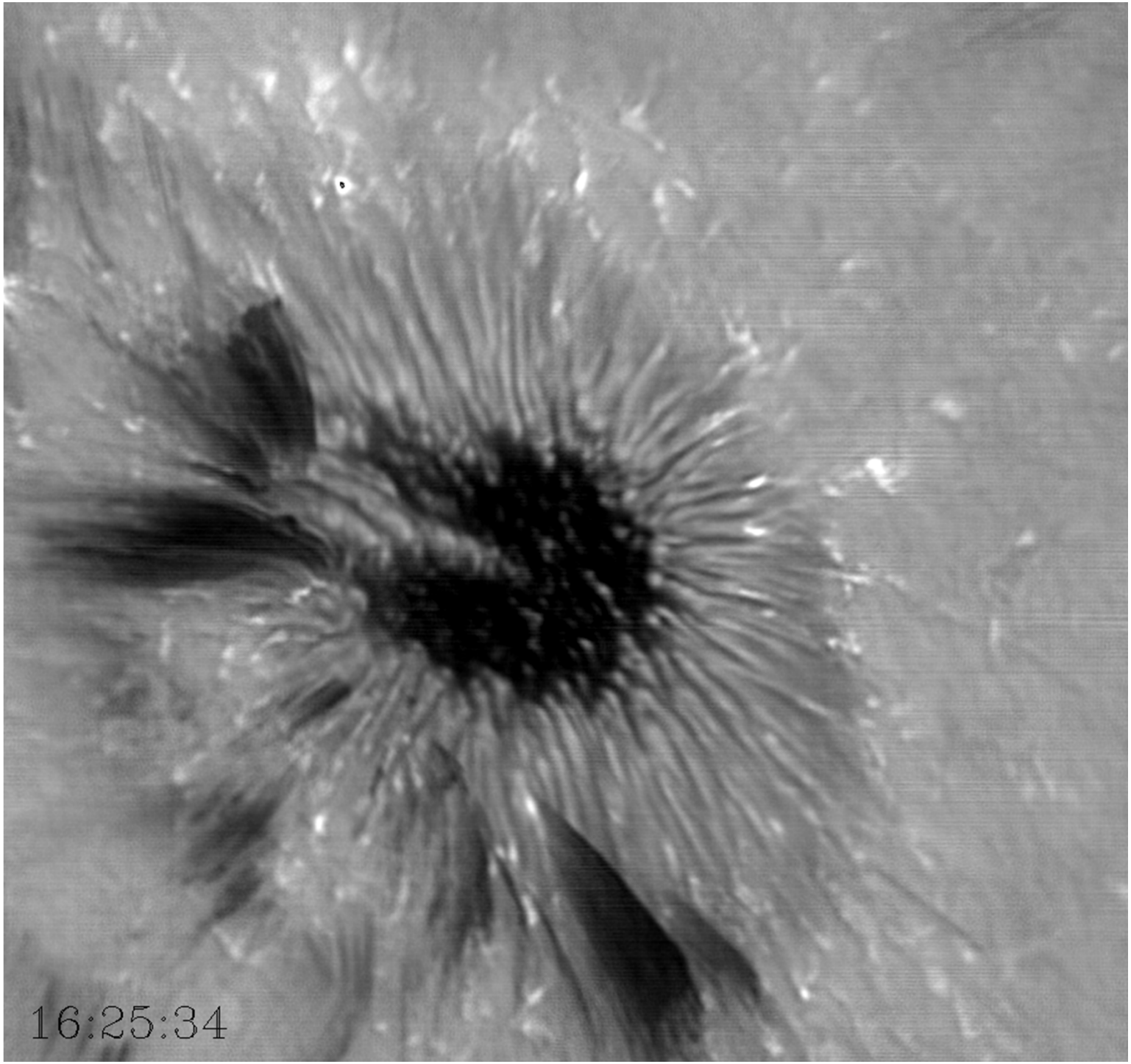

Sunspot atmospheric structure and dynamics

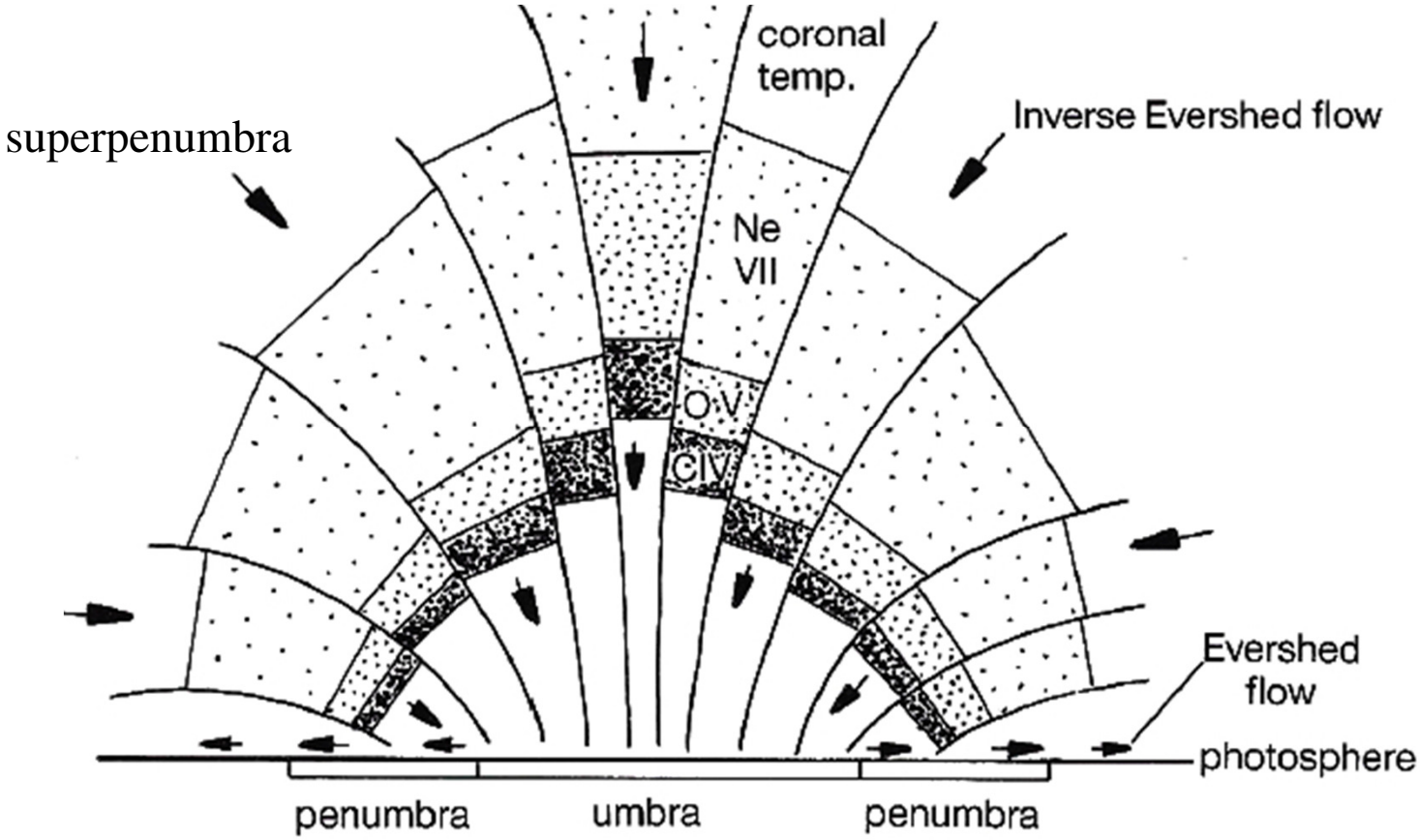

(Nicolas, 1981)